energies

MDPI

Review

Lithium Battery Degradation and Failure Mechanisms: A State-of-the-Art Review

Joselyn Stephane Menye *, Mamadou-Baïlo Camara * and Brayima Dakyo

GREAH Laboratory, University of Le Havre Normandie, 75 Rue Bellot, 76600 Le Havre, France
* Correspondence: joselyn-stephane.menye@univ-lehavre.fr (J.S.M.); mamadou-bailo.camara@univ-lehavre.fr (M.-B.C.)

Abstract: This paper provides a comprehensive analysis of the lithium battery degradation mechanisms and failure modes. It discusses these issues in a general context and then focuses on various families or material types used in the batteries, particularly in anodes and cathodes. The paper begins with a general overview of lithium batteries and their operations. It explains the fundamental principles of the electrochemical reaction that occurs in a battery, as well as the key components such as the anode, cathode, and electrolyte. The paper explores also the degradation processes and failure modes of lithium batteries. It examines the main factors contributing to these issues, including the operating temperature and current. It highlights the specific degradation mechanisms associated with each type of material, whether it is graphite, silicon, metallic lithium, cobalt, nickel, or manganese oxides used in the electrodes. Some degradations are due to the temperature and the current waveforms. Then, the importance of thermal management and current management is emphasized throughout the paper. It highlights the negative effects of overheating, excessive current, or inappropriate voltage on the stability and lifespan of lithium batteries. It also underscores the significance of battery management systems (BMS) in monitoring and controlling these parameters to minimize the degradation and the risk of failure. This work provides a summary of valuable insight into the development of BMS. It emphasizes the importance of understanding the degradation mechanisms and failure modes specific to different families of lithium batteries, as well as the critical influence of temperature and current quality. Rational management or efficient controlling of these parameters can enhance the performance, reliability, and lifespan of lithium batteries.

Keywords: lithium-ion battery; battery degradation and failure; battery management systems; battery aging; battery characterization

check for updates

Academic Editors: Cheng Zhang, Truong Minh Ngoc Bui and Truong Quang Dinh

Received: 12 November 2024
Revised: 12 December 2024
Accepted: 8 January 2025
Published: 14 January 2025

Citation: Menye, J.S.; Camara, M.-B.; Dakyo, B. Lithium Battery Degradation and Failure Mechanisms: A State-of-the-Art Review. *Energies* **2025**, *18*, 342. https://doi.org/10.3390/en18020342

Copyright: © 2025 by the authors. Licensee MDPI, Basel, Switzerland. This article is an open access article distributed under the terms and conditions of the Creative Commons Attribution (CC BY) license (https://creativecommons.org/licenses/by/4.0/).

1. Introduction

Lithium-ion batteries (LIBs) are used in many applications ranging from portable electronics to electric vehicles (EVs), as well as renewable energy installations, where they enable better deployment and energy management between the production systems and energy requirements. However, their performance and safety are often compromised by degradation mechanisms and failures, raising concerns for users and manufacturers. Understanding these processes is essential not only to optimize the reliability of LIBs but also to guide the development of innovative and sustainable solutions. This paper aims to gather and synthesize existing knowledge on the chemistry and operation of LIBs, as well as on methods for estimating their state of health (SOH).

Considering the impact of electrical and batteries using conditions such as state of charge (SOC), depth of discharge (DOD), and temperature, we shed light on the challenges

associated with battery health. By identifying gaps in current research and directing future studies toward strategies for mitigating degradation. This work contributes to a better understanding of the issues related to LIBs. In doing so, it offers practical insights for engineers and researchers, promoting safer usage practices and the development of more robust battery technologies, which are essential for the development of widespread and sustainable energy systems.

The structure of this paper is as follows: Section 2 discusses lithium battery technology, detailing its structure and operation, with particular emphasis on the chemistry and various technologies available on the market. Section 3 briefly covers cycling methods and SOH estimation techniques. It focuses more on the degradation and failure of lithium batteries, examining their causes as well as the influences of various parameters that can affect SOH, such as electrical quantities, temperature, charge level, and mechanical stress. Finally, Section 4 addresses the role of Battery Management Systems (BMS) in preventing and anticipating degradation and/or failure modes of LIBs, emphasizing their crucial role in maintaining battery health.

2. Lithium-Ion Batteries Operating Principle

The failure of lithium-ion batteries (LIBs) is primarily attributed to three main aspects: the nature of the materials used, the rigor in design and manufacturing, and finally, the influence of the operating environment. To better understand these degradation processes and address the major challenges that persist in the field of energy storage with LIBs, it is essential to gain a deeper insight into their operation and the key materials that make up LIBs.

The basic operating principle of LIBs is illustrated in Figure 1. The functioning of a LIB can be summarized by the charging and discharging processes, which are driven by electrochemical reactions (Equations (1) and (2)).

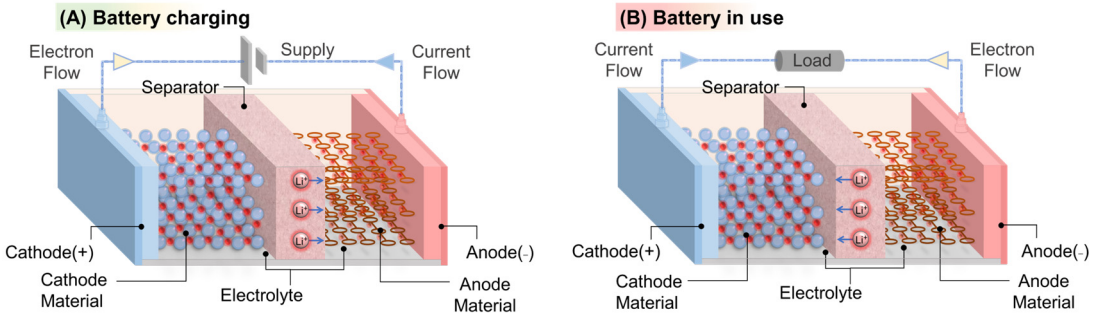


Figure 1. Operating principle of a lithium-ion battery (LIB).

- During charging: Electrical Energy → Chemical Energy
  Lithium ions move from the cathode to the anode, where they are intercalated into the anode material. The general equation can be written as follows:

$$Li_xM^{n+} + ne^- \rightleftharpoons Li_yM \quad (1)$$

where

- Li_xM^{n+} represents the oxidized form of the cathode material (where M can be a metal, such as cobalt or nickel);
- n is the number of electrons transferred;
- Li_yM represents the reduced form of the anode material.

- During discharging: Chemical Energy → Electrical Energy
  Lithium ions move back from the anode to the cathode, releasing electrical energy. The general equation can be expressed as follows:

$$Li_yM \rightleftharpoons Li_xM^{n+} + ne^- \quad (2)$$

It consists of key components such as the electrodes (anode and cathode), which serve as an "energy tank" capable of storing and releasing Li^+ ions, according to the operating mode of the LIB, as well as the separator and the electrolyte.

- Anode: The electrode suitable for oxidation reactions, which is specific to the discharge of the battery. During this process, the anode, through mechanisms inherent to the materials that compose it, releases Li^+ ions to the cathode via the electrolyte. Simultaneously, the electrons move from the anode to the cathode through the current collectors, supplying the load. Most of the materials used in this electrode typically have a capacity greater than that of the cathode;
- Cathode: It is often the most expensive component of the batteries [1]. The choice of cathode materials can optimize several criteria such as energy density, battery capacity, thermal stability, and cost. Cathodes in LIBs are generally composed of intercalation materials, which have the main advantage of undergoing minimal changes to their crystalline structure during the insertion and deintercalation phases of Li^+ ions while the battery operates. Notably, the cathode is the site of reduction reactions, which is the key process during the battery operation. During the charging phases, electrons from the external circuit combine with Li^+ ions from the cathode, which are then stored in the anode.

The separator and electrolyte act as barriers between the two electrodes. The separator is a microporous membrane that prevents short circuits (SC) between the electrodes while allowing ionic transport. It also plays a vital role in the safety of LIBs. Through a phenomenon known as "shutdown", it can prevent failures such as thermal runaway (TR) and SC. There are three main classes of separator materials: (a) modified polymeric separators, (b) composite separators, and (c) inorganic separators [2]. Modified polymer separators, such as polyethylene or polypropylene, are enhanced for ionic conductivity and thermal stability. Composite separators combine various materials to leverage their advantages, providing mechanical and chemical resistance. Finally, inorganic separators, often made from ceramics, are distinguished by their high thermal and chemical stability. Some separators also benefit from a ceramic coating, enhancing their thermal deformation resistance and mechanical strength [3].

The electrolyte, for its part, is an ionic conductor for lithium ions between the electrodes. It must possess several characteristics, including good ionic conductivity, electrode compatibility, low flammability, and significant thermal stability. LIBs use generally two major categories of electrolytes: liquid electrolytes and solid-state electrolytes. Liquid electrolytes are generally the solutions of lithium salts, such as $LiPF_6$ (Lithium Hexafluorophosphate), $LiBF_4$ (Lithium Tetrafluoroborate), or LiTFSI (Lithium Bis (Trifluoromethyl Sulfonyl) Imide), in organic solvents like carbonates or ethers. They offer excellent ionic conductivity but pose safety issues related to the flammability of the solvents. The development of solid-state electrolytes which have been designed to address these safety issues represents a significant advancement in batteries technologies. There are three categories:

- Inorganic solid electrolytes such as ceramics or glass-ceramics, which do not contain flammable organic solvents;
- Gel polymer electrolytes combine the flexibility of polymers with better conductivity than dry polymers;

- Solid polymer electrolytes which have the lower ionic conductivity compared to liquid electrolytes offer the advantages of high mechanical strength and good safety [3,4].

Finally, hybrid electrolytes have also been designed, leveraging the combined benefits of liquid and solid electrolytes. The choice of the electrolyte is critical as it must be compatible with used materials in the electrodes and the operating conditions of a battery. These different components are illustrated in Figure 2 [5–13].

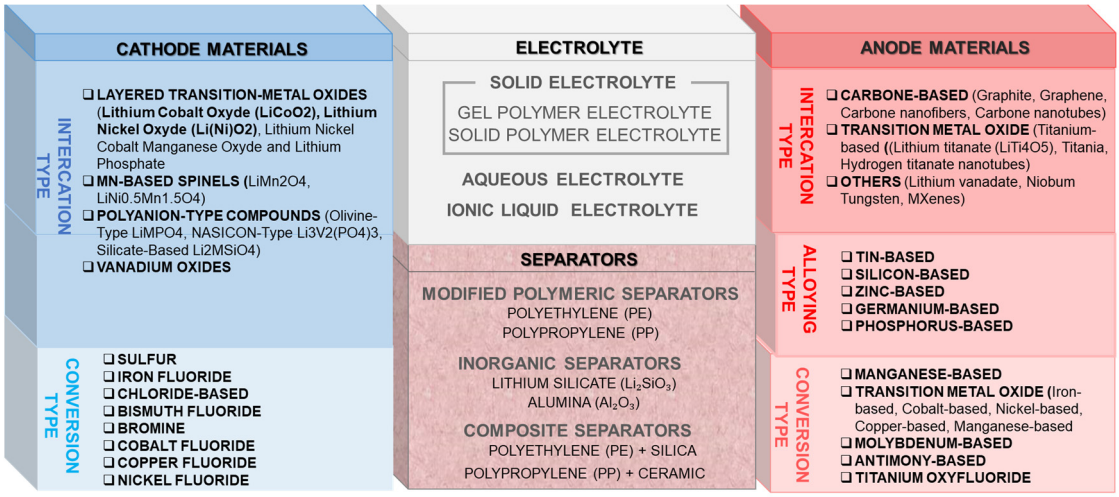


Figure 2. Overview of various materials of LIBs.

LIBs operate through a variety of mechanisms due to the nature of the electrode materials and the electrochemical reactions involved. As shown in Figure 2, the lithium storage and release mechanisms in the electrodes are influenced by the type of redox electrochemical reactions at play. Depending on the active materials of the electrodes, we can observe different types of mechanisms such as the follows:

- Intercalation/Deintercalation mechanisms: The electrode materials act as hosts to accommodate Li ions in a highly ordered one-, two-, or three-dimensional structure. These materials offer significant advantages regarding Li^+ ion transport and cycle life [14,15]. Electrode materials based on intercalation reactions typically have a relatively low theoretical specific capacity compared to materials associated with other mechanisms;
- Alloying mechanism: During charging, these materials form alloys with lithium, resulting in a high reversible capacity, theoretically accommodating 4 or 3 Li^+ ions [14]. Alloy-type materials, such as silicon, tin, phosphorus, and germanium, exhibit high reversible capacity but face significant volumetric changes, as well as issues with structural stability and conductivity (except for germanium, which has a conductivity 10,000 times higher than that of silicon [16]). Alloy-type anode materials generally suffer from significant volumetric changes, leading to capacity loss [14]. These challenges underscore the need for further research and innovation in LIBs;
- Conversion mechanism: This mechanism relies on reversible redox replacement reactions between Li^+ ions and transition metal cations to store lithium [17,18]. This involves lithium reacting irreversibly with certain compounds, such as oxides or sulfides, to form metallic nanoparticles. The reverse process occurs during charging, leading to the original compounds' reformation. However, this mechanism is less reversible than the intercalation mechanism, which can sometimes result in capacity loss after the initial use cycles. What is intriguing is that, like alloy-type materials, conversion-type materials also possess a high theoretical capacity.

Intercalation-type materials offer better cycle life and reversibility but have a lower energy density. On the other hand, alloy and conversion-type materials exhibit much higher capacities but with variable stability. In general, LIBs use intercalation-type materials. The various active materials for the cathodes associated with this mechanism are distinguished by their advantages and disadvantages in terms of cycle life, cost, energy density, and other criteria. These materials in cathode are generally categorized into three types: (a) layered oxides, (b) spinel oxides, and (c) olivine polyanions [19]. Phosphate-based cathodes such as LFP (Lithium Iron Phosphate) are thermally stable but have low intrinsic electric conductivity, which a carbon coating improves. Spinel oxide-based cathodes such as LMO (Lithium Manganese Oxide) and LNMO (Lithium Manganese Nickel Oxide) are less expensive as they do not use cobalt but have a higher operating voltage and lower capacity than layered oxides. Among these, NMC (Nickel Manganese Cobalt) and NCA (Nickel Cobalt Aluminum) materials are the most widely used in EV applications, with NMC offering a better balance of cost and stability. Additionally, NMC cathodes have a longer lifespan than polyanion and spinel cathodes [20,21].

It is important to note that many electrode materials and electrolytes are not currently commercialized, which highlights the need for Tables 1 and 2, which present the most widely used electrodes on the market. There is a wide range of chemical compounds that are used as positive electrodes, particularly for common materials such as LCO, LMO, NMC, NCA, LNMO, and LFP [22–26].

Table 1. Most common cathode materials.

Structure Category	Cathode Materials	Merits	Remarks	Practical/Theoretical Capacity (mAh·g^{-1})	Potential (V vs. Li/Li$^+$)
Olivine	LFP	Lower cost; good stability during rapid charge/discharge; good stability against heat and rapid charge; long lifespan	Lower energy density; limited high-rate charging	160/170	3.2–3.7
Layered	LCO	Highest energy density; good stability during charge and discharge	Rapid capacity loss at high temperatures	145/274	3.0–4.5
	NMC811	High energy density; good stability during charge and discharge	Higher sensitivity to temperature	200/276	2.5–4.6
	NMC622	High energy density; good stability during charge and discharge		185/277	3.7–4.2
	LMR-NMC	High energy density		250/277	3.5–4.8
	NCA	High energy density; good stability during charge and discharge	Higher sensitivity to temperature; higher cost compared to other types	200/279	3.0–4.2
Spinel	LMO	Moderate energy density; lower cost, good stability during rapid charge and discharge	Rapid capacity loss over time	120/148	3.0–4.3
	LNMO	Stable spinel structure and transition metal stoichiometry promote fast Li uptake, enabling high rate capability and an elevated operating voltage (≈4.7 V vs. Li$^+$/Li)	LNMO may significantly lose capacity during cycling due to Mn diffusion in the electrolyte from Jahn–Teller effect modifications	140/147	3.5–4.8

A dominant solution for anode material in LIBs is carbon (graphite), which is recognized for its high specific capacity and low volumetric expansion. Graphite's ability to facilitate the insertion and extraction of Li^+ ions, combined with a low rate of irreversible loss, makes it a benchmark compound in the LIB industry, contributing to better cycle life and overall performance in conventional LIBs [14,27]. Lithium Titanate Oxide ($Li_4Ti_5O_{12}$ (LTO)) anodes available on the LIB market represent a very promising alternative to carbon-based anodes. Their nanoscale crystalline structure enables rapid ion extraction during charging [28].

Table 2. Most common anode materials.

Anode Type	Anode Materials	Theoretical Capacity ($mAh \cdot g^{-1}$)	Merits	Remarks
Intercalation-Type	Carbon-based Nanostructures (CN)	1000–1200	CN has been proposed to address excessive volumetric fluctuations, low cycling stability, limited faradaic efficiency, insufficient ionic, and instability of the SEI. They provide excellent mechanical properties and high thermal conductivity [29,30].	CN has a lower apparent density compared to graphite anodes, which reduces the volumetric capacity of these electrodes. Most CNs with high specific capacity are limited to thin film dimensions, making them unsuitable for large-scale applications [31].
	Graphite	372	The material offers a low stable discharge voltage platform and good cycling ability, along with advantages such as low cost, abundant resources, and stable, reversible electrochemical performance compared to lithium [15,32].	The lithium-storage capacity is insufficient for electric device demands, and the slow diffusion rate of lithium ions leads to poor performance for graphite electrodes. Furthermore, the material has a low operating potential (<0.1 V) and a high lithium ion diffusion coefficient, ranging from 10^{-9} to 10^{-7} cm^2 s^{-1} [32,33].
	Graphene (soft carbon)	744	Like graphite, it offers excellent rapid charge–discharge cycles and a higher lithium-ion storage capacity. With a specific surface area of 2620 m^2/g, it also demonstrates outstanding mechanical strength, thermal conductivity, and good electron mobility of 15,000 $cm^2/V \cdot s$ [34].	Low stability and ionic steric influence [34]
	Hard Carbon	200–600	Excellent working potential and excellent cyclability [35].	Low columbic efficiency [35].
	LTO (spinel-framework structure)	170	Low cost, negligible volume expansion, high thermal stability, can operate at low temperatures [36].	Lower voltage level than the other Li-ion battery chemistries [36]

Another anode material that is generating significant interest is silicon. Despite the challenges it faces, with alloy-type mechanisms during the lithiation/delithiation process. Its specific capacity is more than ten times compared to commercial graphite anodes. The theoretical specific capacity of $Li_{15}Si_4$ formed with lithium ions at room temperature of 20 to 25 °C, is about 3580 mAh g^{-1}, while the specific capacity of $Li_{22}Si_4$ formed with lithium ions at elevated temperatures (400 to 700 °C) is 4200 mAh g^{-1}. It is imperative to note that silicon is currently one of the anode materials with the highest specific capacity. In addition to its very high specific capacity, silicon has a natural abundance and an appropriate working potential, making it one of the most promising anode materials to meet the increasing energy density requirements of LIBs. However, the silicon anode faces several major challenges due to the significant volume expansion of silicon (~300%) during battery operation [37].

To achieve the required voltage, cells can be connected in series and generally come in three geometries: cylindrical, prismatic, and pouch (Figure 3). Each of these cells has distinct structures, performances, and applications [38]. The choice of format influences various parameters, such as pack design, energy density, cooling systems, and safety [39].

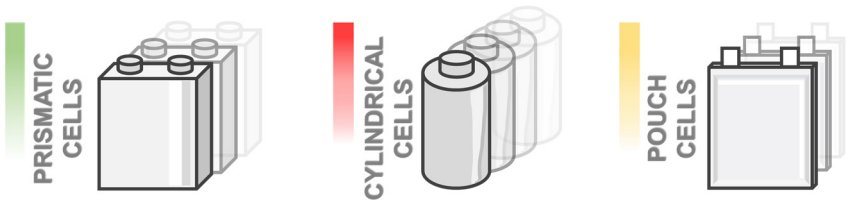


Figure 3. Different geometries of battery cells.

Figure 4 provides a comparative overview of the design properties of popular Li-ion battery configurations, showing that the cylindrical cell offers good cost-effectiveness and flexibility in system construction. Pouch cells, on the other hand, are lightweight and flexible but have limited mechanical durability and can easily swell due to gas buildup. They can take various shapes, not just their well-known rectangular form. Cylindrical cells, typically wound in steel casings, provide good energy density and effective thermal management, although their format (such as 18,650 and 21,700) can be limited. Prismatic cells benefit from higher energy density due to better arrangement of active materials and require fewer connections, making them cost-effective to assemble, though their mechanical integrity is direction-dependent [40–43].

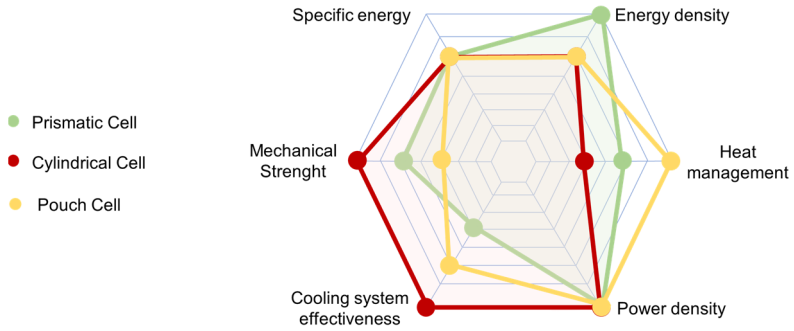


Figure 4. Comparison between properties of standard lithium-ion cell designs—this figure is adapted from [43].

Between 2010 and 2021, all formats saw continuous performance improvements, with pouch cells reaching around 560 Wh/L, thus surpassing cylindrical cells, which doubled their capacity to about 4.5 Ah. Prismatic cells also progressed, increasing from 60 Ah to 150 Ah, particularly thanks to LFP-based cathodes, with an average energy density of 400–450 Wh/L [38]. The performance differences among these formats are related to the active materials and the proportion of components in each cell.

The composition and form of the batteries play a crucial role in the failure and aging of LIBs. Based on Bugryniec et al.'s work, several conclusions can be drawn, such as the following: (a) NMC LIBs generate larger specific volumes of emitted gas than other chemistries; (b) prismatic cells tend to produce higher specific gas volumes than other configurations; and (c) LFP batteries exhibit more significant toxicity than NMC batteries [44]. However, the influence of usage and non-usage conditions remains predominant.

3. Failures and Degradations of the Lithium-Ion Batteries

3.1. Testing Methods and End-of-Life Evaluation

Batteries are usually degraded over time due to calendar aging and cyclic aging, which reduces their performance and capacity. Several studies on degradation mechanisms related to calendar aging are proposed in the literature [45–48], but they remain limited due to the required long observation periods. These limitations highlight the important role of accelerated testing, such as high-rate aging tests (HRAT), high-temperature aging

tests (HTAT), or a combination of these last ones. These tests enable a quicker and more accurate evaluation of the impacts of usage and environmental conditions on the state of health (SOH) or the state of charge (SOC) of batteries. Battery is generally considered at the end of life (EOL) when its capacity has decreased to 80% of its original value. This 80% threshold indicates the degree of degradation of the battery over time. Figure 5 shows some approaches to evaluate levels of battery aging. Improving SOH estimation methods and optimizing the battery's performance and lifespan requires a deep understanding of LIB's degradation and failure mechanisms.

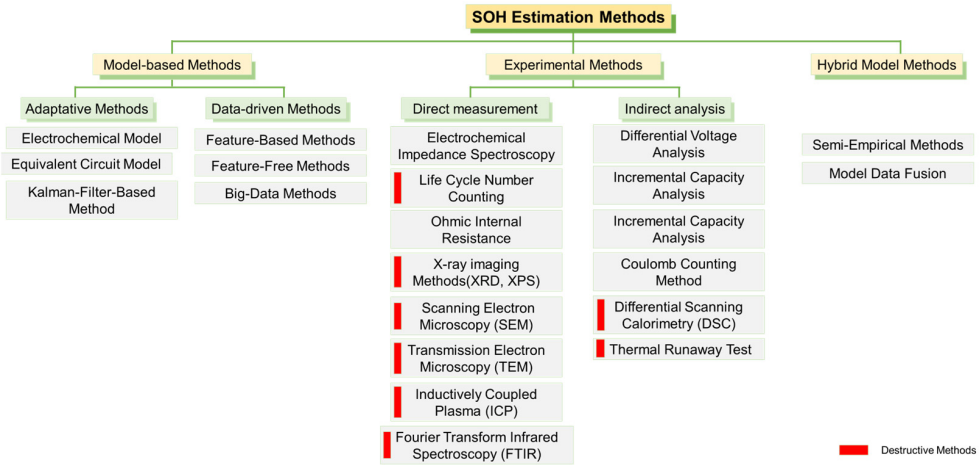


Figure 5. LIB state of health estimation methods.

While Figure 5 provides an overview of various methods for estimating the SOH of batteries, it is crucial to explore other innovative approaches that improve the accuracy of degradation prediction. Deng et al. [49] proposed a method for predicting battery capacity degradation in EVs using field data from 20 commercial vehicles over 29 months. They calculated capacity based on charging data, applied statistical techniques to reduce errors, and analyzed correlations to identify relevant input variables. Using a "Seq2Seq" model enhanced by Gaussian process regression (GPR) for error compensation, this approach showed greater robustness and accuracy compared to traditional methods.

3.2. Aging and Failure Mechanisms

SOH of a LIB is directly linked to the cell's aging and can be interpreted and observed in two main ways. The first approach treats the LIB as a black box, in this configuration, the battery stresses due to the (temperature, current, SOC, etc.) and their impacts on the battery's capacity, power, thermal runaway, etc. are considered. In this case, the SOH is reflected by easily observable or measurable degradation mechanisms such as capacity fade and power fade, as well as failure mechanisms like TR and SC. These two observations are illustrated in Figure 6. At the center of this figure, a LIB is subjected to various external stresses, leading to internal mechanisms that may cause aging or failure of the LIB.

The second approach considers the battery as a white box. This perspective primarily focuses on three modes of degradation: Loss of Active Materials (LAM), Loss of Lithium Inventory (LLI), and Conductivity Loss (CL). These three modes result from underlying mechanisms triggered by external stresses such as temperature, current, or SOC.

- Loss of Lithium Inventory (LLI): This can occur due to the growth of the Cathodic Electrolyte Interphase (CEI) film, electrolyte decomposition, and the growth, decomposition, and regrowth of the Solid Electrolyte Interphase (SEI) film. During lithiation/delithiation, some Li^+ ions are consumed in parasitic reactions, such as the SEI on the negative electrode and the CEI on the positive electrode. While these

passivation layers help "protect" the electrodes from the electrolyte, they tend to thicken overcharge/discharge cycles, trapping more lithium ions and decreasing the LIB's capacity and power;

- Loss of Active Materials (LAM): This refers to the loss of the active mass in the electrodes. This phenomenon can stem from various degradation mechanisms, such as lithium plating/dendrite formation, binder decomposition, corrosion of the current collector, electrode particle cracking, structural disordering, and transition metal dissolution [50–52]. LAM mainly affects positive electrodes, leading to physical damage such as structural disordering of the oxide, dissolution of metal ions, and surface cracking. High voltages and temperatures exacerbate this phenomenon. Dissolved species may interact with the negative electrode or precipitate on the positive electrode, thereby reducing capacity;
- Conductivity Loss (CL): This describes the decrease in the ability of materials to conduct lithium ions and electrons. Such degradation can be caused by binder decomposition, the formation of lithium dendrites, as well as changes in porosity and separator integrity. The consequences include the battery's capacity reducing, internal resistance increasing, and the battery's life decreasing.

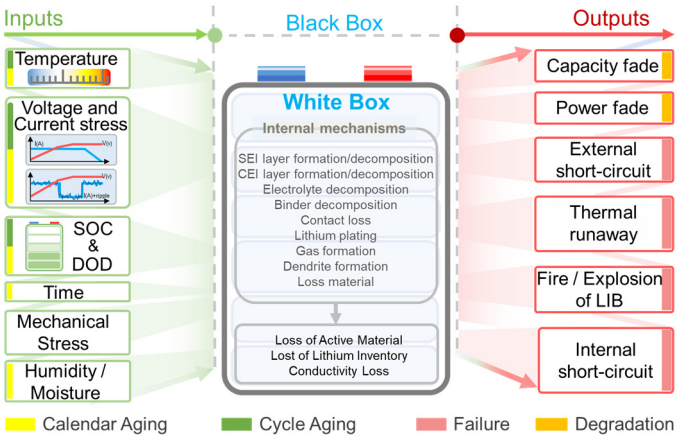


Figure 6. Cause and effect of the battery's degradation and failure mechanisms.

The three main aging modes of the batteries which lead to degradation and possibly failure are significantly influenced by the time, the temperature, the electric, and mechanical stresses. Depending on whether a LIB is in use, these mechanisms can be classified into cyclic aging effects and calendar aging effects.

3.3. Causes and Influences of Aging Mechanisms

Degradation mechanisms present a crucial challenge for various LIB technologies. Understanding the causes and influences of the aging mechanisms is essential for improving the durability and safety of the batteries. The following subsections discuss the key factors that can contribute to the degradation and possibly the failure of LIBs.

Several parameters related to electric current influence the aging of the batteries. The current density or the charge rate has a direct impact on the kinetics of electrochemical reactions, with high values potentially leading to polarization phenomena and dendrite formation, thus accelerating aging. The charge and discharge protocol, with excessively intense cycles or a lack of rest time, imposes the batteries the mechanical and chemical stresses that degrade the active materials and interfaces. Finally, current ripples can induce localized stresses, promoting the emergence of hot spots, which also contribute to fast

aging. Mastering these various aspects related to electric current is therefore essential for optimizing the battery's performance and lifespan.

(a) Current density or Charge/Discharge rate

The current density defines the amount of electric current delivered or absorbed by the battery per unit area of its electrodes. It provides insight into the battery's ability to store energy. Current density is closely related to the charge/discharge rate. Indeed, a variation in the charge (or discharge) rate results in a proportional change in current density. The current density management through the charge rate is essential for optimizing the batteries performances and preventing premature degradation.

The relationship between charge rate and SOH is critical in understanding battery degradation. Gailani et al. [53] highlight the significant impact of the current on the performance's degradation of NMC-Batteries. The higher discharge currents used to stress the cell (high C-rate), the faster the power fade will occur over cycles (Figure 7a). The work of Hao et al. [54] was based on incremental capacity analysis (IC) techniques with NMC- batteries confirms. Those subjected to a charge/discharge rate of 1C/1C (where 1C corresponds to a rate of 2500 mAh) could complete 172 cycles to reach 20% of their SOH, while those cycled at a rate of 2C/2C could only achieve this in 81 cycles for the same result (Figure 7b). These outcomes emphasize that batteries subjected to charge/discharge rates of 1C/1C and 2C/2C perform 1.53- and 3.25-times fewer cycles, respectively, to reach the same 20% SOH compared to a battery subjected to an asymmetric charge rate of 1C/2C for the same goal. This suggests that an asymmetric charge/discharge profile may be more optimal than a symmetric one.

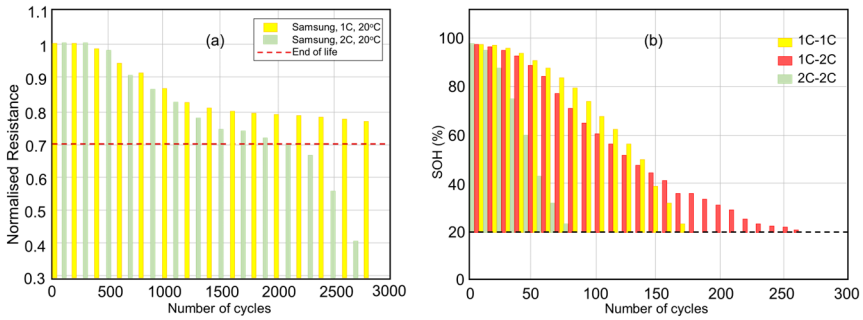


Figure 7. (**a**) Variation in internal resistance for different c-rate, (**b**) impact of the c-rate on SOH.

Different LIB's technologies respond differently to charge rates, emphasizing the need to choose the appropriate technology for specific applications. Gailani et al. [53] examined the calendar and cycle aging of various battery technologies: (a) Samsung SDI AIO 5.5, NMC (94 Ah; prismatic type, 173.2 mm × 45.2 mm × 175.8 mm); (b) Sony US26650, LFP (cylindrical type, diameter: 26.45 mm, length: 65.6 mm); and (c) BYD, LFP (25 Ah; 3.2 V, prismatic type, 173 mm × 21 mm × 119.5 mm). After 18 months at 35 °C and a constant charge rate of 1C, the BYD cells show a 5% increase in resistance, while the Sony cells exhibit the highest increase at 25%. Although the study covers various chemistries and manufacturers, the tests are conducted under controlled conditions, overlooking certain parameters such as humidity and storage duration. Additionally, the differing battery shapes (cylindrical vs. prismatic) may lead to potential biases in the results. Certainly, conductivity is related to the surface area as outlined in Equation (3):

$$R = \rho \frac{L}{A} \tag{3}$$

A = area of the cell; L = length of the cell; ρ = resistivity.

Yuliya Preger et al. [23] examine the influence of the discharge current density (0.5 C, 1 C, 2 C, and 3 C) on the long-term degradation of the many commercial battery's cells: LFP (1.1 Ah, 3.3 V), NMC (3 Ah, 3.6 V), and NCA (3.2 Ah, 3.6 V). Capacity loss decreased with increasing discharge rates for NCA cells, but there was little dependence on discharge rate for NMC and LFP cells. The phenomenon observed in NCA cells by Yuliya Preger et al. [23] is also noted in a study by Dawei Cui et al., which found that the cycling performance (capacity retention) of 18,650 NCA battery cells (2.75 Ah; 3.65 V) was better at a discharge rate of 2 C and 1.5 C at 25 °C.

Other studies have established the influence of operating current on heat generation. Indeed, Shuping Wang et al. [55] study the impact of operating current on the performance and safety of NMC batteries. Figure 8a shows that the heat production during the constant voltage (CV) charging phase increases linearly from 0.075 kJ to 3.12 kJ as the charge current increases from 1 A to 6 A. Total heat generation during charging increases with current but slightly decreases for 6 A compared to 5 A, as the shorter charging time dilutes the effect of the higher current. Figure 8b indicates that the total heat production and residual heat (absorbed by the battery) increase with the discharge current. The share of residual heat is only 5–6% at 1–2 A, but reaches 20% at 6 A, meaning that as current increases, an increasingly significant portion of the generated heat is absorbed by the battery itself, representing more than one-fifth of the total heat production at 6 A. This absorbed heat creates significant temperature gradients within the battery, potentially leading to issues of thermal inhomogeneity and safety during operation.

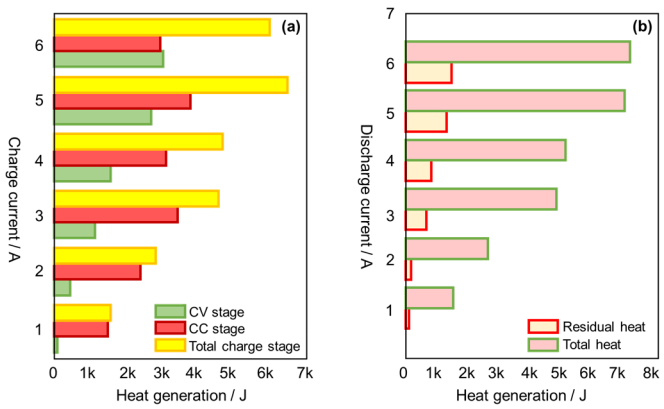


Figure 8. (**a**) Influence of the charge current density in heat generation; (**b**) Influence of the discharge current density in heat generation [55].

In a study considering the LIB as a black box [56], researchers employed a specialized cell design with deformed separators to create controlled non-uniform transport scenarios, aiming to study transitions between no deposition, localized deposition, and homogeneous deposition as the current density in LIBs increased. They concluded that increasing current density promotes localized lithium deposits, which degrades the battery's performance, particularly its capacity.

Barcellona et al. [57] analyze the impact of the current rate on the battery's aging, conducting tests while maintaining the battery's temperature within a safe range and limiting variations in SOC and voltages during cycling tests. This approach allows for the separation of the temperature increase effect from the current rate effect on aging. Based on the results, the authors conclude that the current rate does not directly affect capacity loss during cycling above 95% of the initial capacity for moderate current rates within a limited SOC range and a temperature interval between 20 °C and 30 °C. Following these studies, high charge density would not be a direct cause of cyclic aging in LIBs. However, it can lead to localized fragmentation of particles, potentially resulting in greater stresses [58,59].

To better understand LIB performance and durability in military applications, Wang et al. [60] investigated the degradation of these batteries under various discharge profiles, particularly in ultrahigh conditions. Three A123 LFP/graphite 26650M1B batteries, with a nominal capacity of 2.5 Ah and a maximum discharge current of 70 A, underwent cyclic aging tests at discharge rates of 20 C and 1 C. The results showed that batteries subjected to ultrahigh discharges (Cell C20# and Cell P20#) degrade much faster than those under standard conditions (Cell D5#). For instance, Cell C1# retains 96% of its SOH after 900 Ah, while Cell P20# drops below 80% SOH. Additionally, the internal resistance increases significantly under ultrahigh discharges; at 80% SOH, the resistance of Cell P20# is three times that of a new battery. A peak decomposition analysis reveals that Cell D5# primarily suffers from LLI, while Cell P20# shows significant LAM and signs of lithium plating, indicated by a new peak in its incremental capacity curves. In conclusion, degradation modes differ considerably: Cell D5# experiences linear degradation due to LLI, whereas Cells C20# and P20# exhibit more complex degradation patterns. Elevated temperatures during ultrahigh discharges exacerbate these effects, highlighting the importance of this research for optimizing battery design in critical applications.

The stresses imposed by various lithiation/delithiation mechanisms and temperature variations can cause localized cracks in the active materials of Li-ion batteries, as observed in experiments [61–63]. These cracks represent one of the internal degradation mechanisms of the LIBs. They increase the surface area available for the dissolution of active materials and the formation of the SEI [64]. A relationship has been established between the decrease in capacity of a LIB and the scan rate, and thus the energy density. Indeed, the capacity of the LFP cells decreased progressively from 149 mAh/g to 117 mAh/g at a current density of 30 mA/g [63], a sufficiently high rate to induce internal stresses that could lead to material cracking. This demonstrates that the lifespan of the LIB cells also depends on the "guarantee" of the structural integrity of the host electrodes during charge and discharge.

(b) Influence of current in the Charge/Discharge protocol

Generally, during experimental tests, the operation of the battery is governed by the charge and discharge protocols. The most commonly used charging protocol is the constant voltage (CV)/constant current (CC) method. A direct current (DC) is applied to the battery, gradually increasing its voltage. This step is followed by a constant voltage phase during which the charging voltage is maintained at a predetermined value, while the current gradually decreases as the battery charges further. This allows for a complete and accurate charging of the battery. For the discharge protocol, it is generally simpler. It involves a CC discharge where a CC is maintained at the output of the battery. Discharge continues until the battery voltage reaches a predetermined cutoff value, at which point it can be stopped to avoid excessive discharge and protect the battery.

Many studies describe the influence of the different charge/discharge protocols, using CC-CV or CC protocols as summarized in Table 3. This table summarizes the effects (temperature increase and lifespan) caused by different impulse charging models, using CC and CC-CV charging models as a reference.

The distinct feature of pulsed current protocols lies in the presence of relaxation times. In this context, the work of Haichao Lv et al. [79] highlights the importance of the relaxation time t_{off}. According to the study, increasing the duration of relaxation promotes the uniform distribution of the lithium ions and reduces secondary reactions. These mechanisms positively impact the battery capacity retention rates.

Table 3. Overview of various current mode's effects.

References	Technology	Current Mode	Compared to	Temperature Arise	Lifetime
F. Savoye et al. [65]	LFP	APC	CC-CV	×	×
Y.-D. Lee and S.-Y. Park [66]	LFP	SRC	CC	√	×
M. Abdel-Monem et al. [67,68]	LFP	NPC-CV	CC, CC-CV	×	√
P. Keil et al. [69]	NMC, LFP, LCO	PCCC	CC-CV	×	√
M. Uno and K. Tanaka [70]	LCO	APC	CC-CV	×	√
J. Li et al. [71]	LCO	NPC	CC	×	√
S.-Y. Cho et al. [72]	-	PPC, PPC-CV, SRC-CV	CC, CC-CV	√	×
Chen et al. [73]	NMC	PPC	CC-CV	√	×
		SRC			√
A. Bessman [74]	NMC	SRC	CC	×	√
R. Kannan et al. [75]	NMC	PPC-CV	CC-CV	×	√
A. Bessman, R. Soares [76]	NMC	PPC, SRC	CC	√	×
Huang et al. [77]	NMC	PPC, PCCC, NPC, APC	CC	√	×
Althurthi et al. [78]	NCA	PCC	CC	×	×
		SCC		×	=
		SPCC		×	=

Apart from the work of Haichao Lv et al., the advantages conferred by the pulsed current are further explained by Jia Guo et al. [80], where the charging with pulsed mode inhibits the reduction reaction between the solvent and electrons at the interface. This balances the distribution of Li^+ ions in the electrolyte and reduces lithium depletion at the interface, leading to a thinner SEI layer compared to that produced by the DC. These results account for the reduced increase in interfacial impedance during the charging in the pulsed mode.

Furthermore, numerous studies highlight a correlation between current waveform and dendrite formation, which can lead to phenomena such as internal short circuits (ISC) in LIBs. Indeed, refs. [81–84] demonstrate that pulsed waveforms help reduce dendrite formation. While the current's density influences the increase in internal temperature of a LIB, refs. [85,86] indicate that through a self-heating mechanism, pulsed currents can help regulate the operating temperature of the batteries.

The effects of the pulsed current compared to the DC are described in [65–69] and [87–90]. The various types of pulsed currents are proposed in the literature such as based on frequency, amplitude, and duty cycles. These can be grouped under two categories: PPC (Positive-Pulsed Charging) modes and NPC (Negative-Pulsed Charging) modes (Figure 9). This research identifies pulsation frequency and current amplitude as the most impactful parameters in the degradation of LIBs, where the high frequencies (6 kHz to 100 kHz) show positive effects compared to the low frequencies (1 Hz to 25 Hz).

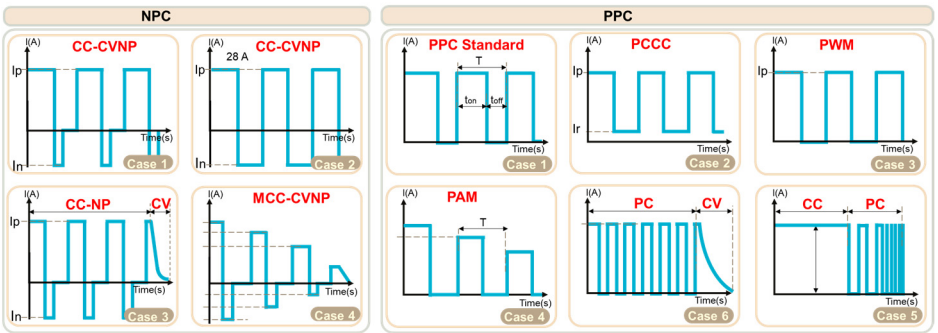


Figure 9. Waveforms of the various charge/discharge protocols [65–69], [87–90].

On the other hand, the amplitude of the pulsed current significantly affects the batteries. Results suggest that increasing the amplitude of the pulses considerably reduces the charging time, but this also leads to a significant decrease in charge capacity and an increase in maximum temperature. Changes in relaxation time had no significant effect on charge capacity or temperature increase. However, a long relaxation time resulted in a long charging duration.

Numerous studies have established the influence of the charge/discharge current on the cyclic aging of LIBs. However, the vast majority of waveforms used for cycling LIBs in the literature still fall short of representing real-world waveforms. To address this, Yunhong Che et al. [91] compare three charge profiles derived from standard test conditions of an EV (Urban Dynamic Driving Profile (UDDS), the Highway Driving Profile (HWFET), and the Hybrid Profile (a combination of UDDS and HWFET)) to the CC profile. These three loading profiles are beneficial for simulating battery operation under urban, highway, and hybrid driving conditions, respectively. Under constant temperature, the HWFET leads to the fastest aging, while the UDDS has the longest lifespan. Under variable temperature conditions, both UDDS and hybrid operating conditions extend the battery life compared to CC and highway conditions.

In this same vein, Kalk et al. [92] study effects of realistic driving profiles on the degradation of LFP (3.2 V, 3 Ah). The tests were conducted at 20 °C using the CC-CV protocol with standard profiles Zyk1 (1C) and Zyk2 (2C), as well as realistic driving profiles ("normal use" and "high use" with fast charging), all tested between 20% and 100% SOC. The Zyk2 protocol showed the slowest aging, reaching EoL after about 11 kAh, while Zyk1 reached it after 8 kAh. In contrast, realistic profiles led to accelerated degradation, with the high-use profile reaching EOL after only 2.4 kAh. Calendar aging was also examined through storage tests at 25 °C with 30% and 100% SOC, showing a decrease in the capacity loss rate over time. Tests with realistic profiles were shorter, reducing calendar aging impact. EIS analysis revealed increased electric losses with ohmic resistance (R_0) increasing less under realistic profiles, possibly due to amplified lithium-consuming degradation processes. This research underscores the necessity of using realistic driving profiles to assess the lifespan of EV batteries, which has implications for improving battery management systems.

(c) Influence of the current ripples

Many studies have aimed to verify the hypothesis that the LIBs undergo a degradation process when exposed to ripples or alternating currents (AC) of varying frequencies. Table 4 summarizes different works that have focused on the influence of the current ripples in the degradation process of LIBs.

Table 4. Overview of current ripple effects on LIBs.

Refs	Materials/Methods	Tests Conditions	Remarks
Brand et al. [93]	18 Li-ion Cells (NMC and anode in graphite). Climate chamber (25 °C)	DC (450 mA) with a superimposed AC of amplitude ±400 mA (30 kHz, 1 kHz, and 1 Hz).	Current studies show that the frequency of the current fluctuations does not influence the battery lifespan as much as expected.
Bala et al. [94]	LFP cathode and Graphite anode	AC frequency: 120 Hz	An AC frequency of 120 Hz was superimposed, resulting in a temperature increase that could lead to accelerated aging.

Table 4. *Cont.*

Refs	Materials/Methods	Tests Conditions	Remarks
K. Bellache et al. [95]	LFP cathode	Study based on 4800 cycle tests, utilizing a frequency range of 50–500 mHz and a temperature range of 10–80 °C.	The average energy capacity of LFP batteries decreases with the increase in the frequency of DC ripples. In contrast, the average resistance of the batteries increases as the frequency of DC ripples rises.
Beh et al. [96]	LFP batteries with 2000 cycles	Pulses and direct current (DC)	The battery's capacity decreases after 2000 cycles by about 15.1% for charging in DC and 16.3% for charging by pulses.
Prasad et al. [97]	800 cycles for LMO batteries	Sinusoidal AC (120 Hz) superimposed	The capacity of the battery charged with sinusoidal current decreased by 3.9%, and by 4.2% for the battery charged in DC
De Breucker et al. [98]	Current ripple originating from a boost converter on the LiPO batteries	Subjected to high AC amplitudes of 40 A or low amplitudes of 1 A.	The study did not manage to demonstrate a significant impact of the current ripple on the aging of the LIB under these test conditions. The absence of an effect from the current ripple on the battery aging could be attributed to the capability of the electric double layer intrinsic to the electrodes. This double layer acts like a capacitor, capable of absorbing part of the HF current ripple.
Uno et al. [70]	LCO LIB	Study of the effect of pure AC with frequencies ranging from 1 Hz to 100 kHz.	The results indicate accelerated degradation for frequencies below 10 Hz. Above 10 Hz, only non-Faradaic processes occur, and no further degradation is observed. Electrochemical processes are activated only at frequencies lower than the corner frequency of the RC elements, which represent the charge transfer resistances in parallel with the Electric Double-Layer Capacitor, and therefore experience faster aging.
Uddin et al. [99,100]	15 NCA cells	Superimposition of AC (0 Hz, 10 Hz, 55 Hz, 254 Hz, and 14.8 kHz).	Capacities decrease and impedances increase more rapidly for battery cells cycled at higher frequencies due to the resulting heating and growth of the SEI.
Goldammer et al. [101]	60 NMC cells (pouch type with a nominal capacity of 50 Ah) with a graphite anode.	Temperature: 25 °C DC; AC Current (10–40 kHz (6.25 A, 12.5 A, 25 A)); Artificial Ripple; Realistic Ripple (WLTC and UDDS);	When 45 Ah is defined as the EOL for the cells, the results indicate a decrease in cell lifespan with AC or ripple currents, with the loss of ampere-hours until EoL varying from 13% to 45%, depending on the type of superimposed current. The capacity fade depends on the amplitude and frequency of the oscillations, with an increase in loss for higher amplitudes and a doubled frequency of 10 to 20 kHz. These observations confirm that ripple currents, generated by semiconductor switching, contribute to significant aging of cells in EV.
Ferraz et Kowal [102]	LG 18,650 HE4′ cylindrical LIB (NMC) with a graphite anode	High-frequency (HF) current ripples	The results suggest that there is little to no additional influence from current ripples that is significant enough to distinguish it from the aging effects caused by the underlying accelerated cyclic aging.

Table 4. *Cont.*

Refs	Materials/Methods	Tests Conditions	Remarks
Chang et al. [103]	5 Panasonic NCR cells ($LiNiCoAlO_2$) subjected to 500 cycles.	- DC (cells 1 and 2) - Ripple current (2 kHz (cell 3), 10 kHz (cells 4 and 5))	- The aging experiment shows that current ripples in the CHB increased the capacity reduction in the battery cells by 2.1%. - The ripples in the CHB do not significantly accelerate the aging of the batteries, regardless of the switching frequency and power factor.
Frenander and Thiringer [104]	2170 cells from a Tesla Model 3 car (Silicon and Graphite/NCA)	Influence of low-frequency (LF) current pulses (f < 100 mHz) and HF current pulses (f > 100 mHz)	- Cells subjected to HF pulses show faster capacity degradation than those with LF pulses. - The degradation of the cells is primarily due to the capacity loss of the negative electrode, particularly the silicon portion of the Si-Gr composite electrode. Previous studies suggest that this is caused by volumetric expansion, leading to fractures in the SEI layer.
Hao Li et al. [105]	4 DC-DC converters generating HF ripples applied to NMC LIBs.	Current ripples of 4 kHz and 10 kHz.	- The HF ripple current slightly accelerates the capacity drop of the anode, which can impact the overall capacity and performance of the battery. However, its effect remains relatively limited compared to the impact of temperature. - The ripple amplitude at 4 kHz has a more significant effect than that at 10 kHz.
Ghassemi et al. [106]	LFP LIB tested at 22–24 °C	0.5 C–0.87 C sinusoidal ripple superimposed on 0.5 C DC at 0.1 Hz, 100 Hz, and 1 kHz	On the basis of the Incremental Capacity Analysis (ICA) and Differential Voltage Analysis (DVA) method, the results show that the LF current ripple accelerates the LLI and LAM of the LIB, while HF current ripple has no significant effect on the battery life degradation

The analyses conducted on LIBs have not led to a single, definitive conclusion. The divergences observed in the interpretation of the results highlight the complexity of this issue and leave the field open for further research. Although the impedance properties of these batteries appear to evolve in a particular manner depending on the SOC. It is important to note that the influence of the current's ripples remains negligible compared to other factors such as the temperature and the charge/discharge mechanisms.

(d) Influence of the voltage

High or low voltage levels can impact the lifespan and performance of batteries. When discussing voltage influence, we mainly refer to capacity variations among individual cells in a battery pack. These differences complicate the maintenance of identical SOC for each cell. Consequently, when cells reach critical charge or discharge levels, they may face extreme conditions that lead to failures, typically manifesting as overcharge and over-discharge issues.

Like other aging causes, overcharging and excessive discharging induce undesirable side reactions within the battery, summarized by the LAM and LLI modes [107]. Over-discharge is closely related to the DOD. Excessive lithium extraction during this phase can cause the cathode to collapse, often accompanied by a significant increase in the heat [108]. On the other hand, overcharging stresses the anode, leading to over-lithiation, which results in increased resistance and degradation of the electrolyte [109].

Zou et al. [110] briefly present the causes and effects of overcharging and excessive discharging, including excessive cooling, overheating, high charge and discharge rates, inconsistency, and other factors, as illustrated in Figure 10.

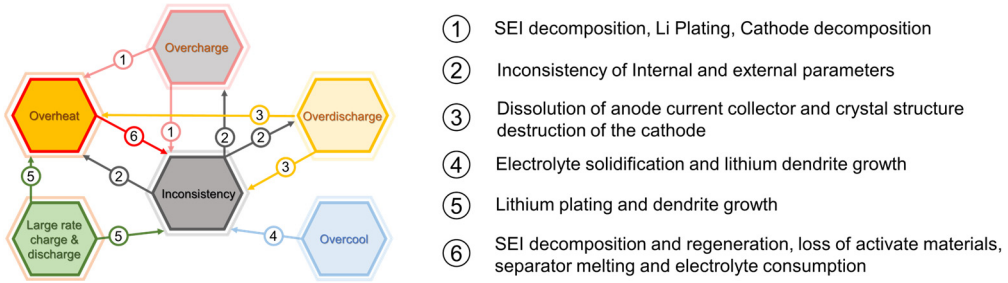


Figure 10. Overview of the causes and effects of overcharge and overdischarge phenomena [110].

Analysis of the electrochemical and thermal behaviors under various conditions of retired power lithium-ion batteries (PLIBs) by Li et al. [111] shows that overcharge and excessive discharge cycles negatively affect the SOH of the batteries. After 800 cycles, the SOH decreases by 6.84% during normal cycles, by 8.12% during discharge cycles, and by 9.44% after only 200 overcharge cycles, reaching 67.52% after 800 cycles. Overcharging leads to a more rapid degradation of performance due to the deposition of lithium ions on the graphite electrode. Furthermore, internal resistance increases, particularly when the SOC drops below 20%, as a result of lithium and electrolyte loss. Overcharge cycles also lead to elevated maximum temperatures, highlighting the necessity of an effective thermal management system to ensure stability. This material loss aligns with the findings of Guo et al. [112], which establishes a correlation between the likelihood of ISC occurrence and both DoD and SOC.

Similarly, Salim Erol [113] explores the impact of excessive discharge and overcharge on 18,650 Graphite/$LiCoO_2$ cells. Impedance spectroscopy was performed at specific potentials, such as 4.20 V for the normal cell and between 2.70 V and 4.70 V under discharge and charge conditions. The results indicate a significant increase in impedance during overcharge and excessive discharge. While ohmic resistance remains stable, capacitance and charge transfer resistances vary, with anodic capacitance increasing at 4.70 V, suggesting electrochemical changes. After excessive discharge, the impedance at 4.20 V is similar to the initial state, suggesting that the effects of discharge are reversible. Conversely, overcharging results in more permanent changes to battery parameters. SEM analysis of the electrodes reveals typical morphology under normal conditions, agglomerations after discharge, and cracks and material losses following overcharge. Notably, all measurements were performed at room temperature and repeated at least three times to ensure consistency and reproducibility of the findings.

Expanding on the analysis of the effects of overcharging, Gotz et al. [114] investigated the combined effects of overcharging (OC) and over-discharging (OD) on 18,650 cells, a topic that has been less explored in the literature. The experiments were conducted using Samsung IRF22P NMC (Nickel-Manganese-Cobalt) 18,650 cells, which have a nominal capacity of 2200 mAh and a voltage of 3.7 V. The results on the discharged capacity of lithium-ion cells reveal a significant impact of overcharging based on voltage thresholds. Cells charged to 4.4 V, 4.5 V, and 4.6 V retained their capacity after three cycles, whereas those charged to 4.8 V lost approximately 6% in the first cycle and over 13% in the second, totaling a 19% loss after two cycles (Figure 11, [114]). The rupture of the current interrupt device (CID) membrane in the fourth cycle resulted in a total loss of capacity. For cells at 5.0 V, the capacity loss occurred immediately during the first cycle.

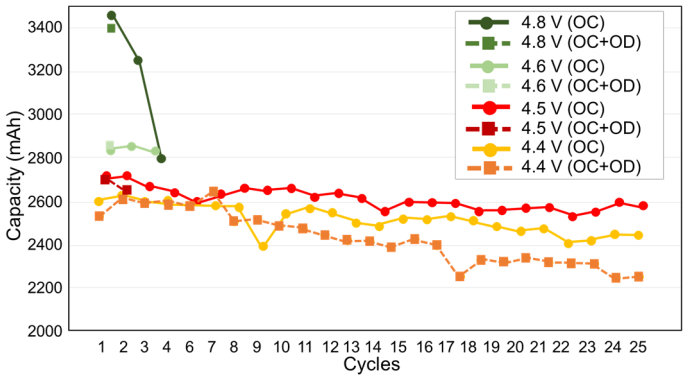


Figure 11. Capacity for cells under OC and OC + OD abuse—this figure is adapted from [114].

The analysis of cells under OC + OD shows that the combination of OC and OD increases the severity of consequences. A cell charged to 4.5 V under OC does not rupture its CID membrane, but the rupture occurs if it is discharged to 1.0 V due to a high oxidation level. The cell at 4.4 V is the only one that did not experience a rupture, although it lost about 11% of its capacity after twenty-five cycles. For the 4.5 V cell, the CID membrane ruptured after two cycles, resulting in a capacity loss from 2716 to 2625 mAh. Cells at 4.6 V and 4.8 V also ruptured their CID membranes after one complete cycle each. These results highlight the importance of carefully monitoring charging and discharging conditions.

(e) Influence of Depth of Discharge (DOD)

DOD represents the fraction of the battery's total capacity that has been used during a charge/discharge operation. In other words, DOD is the percentage of the battery's nominal capacity that has been discharged. It is related to the SOC with the inversely proportional relationship as illustrated in Figure 12 [115].

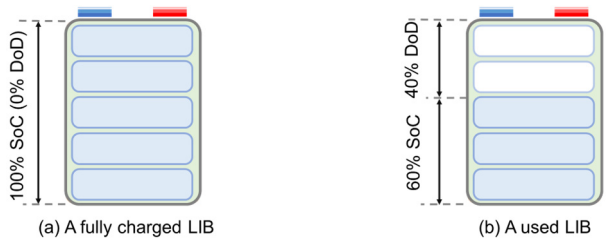


Figure 12. Illustration of the principles of SOC and DOD.

Figure 13a shows that for an LFP cell, a DOD between 60% and 20% causes lower capacity losses compared to a DOD between 85% and 45% [53]. Furthermore, the results highlight the impact of a 10 °C increase in the temperature on capacity loss for the same type of cell, comparable to the level of DOD. The same study shows that among the three cells examined, the Samsung NMC cell exhibited the lowest increase in resistance (around 10%) after 3000 cycles compared to 25% for the Sony LFP cell and 78% for the BYD LFP cell after 2000 cycles. Nevertheless, it is observed that the Sony and BYD cells, with identical chemistry and nominal voltages, do not react similarly to the DOD. If the resistance of the battery after 1000 cycles is greater at a DOD of 80% for BYD cells, that of Sony cells proves to be "significant" at a DOD of 20%. However, overall, the DOD has a lesser impact on the battery's resistance increasing than on their capacity loss under the same operating conditions (Figure 13b–d [53]). These conclusions do not align with those of Yuliya Preger et al. [23].

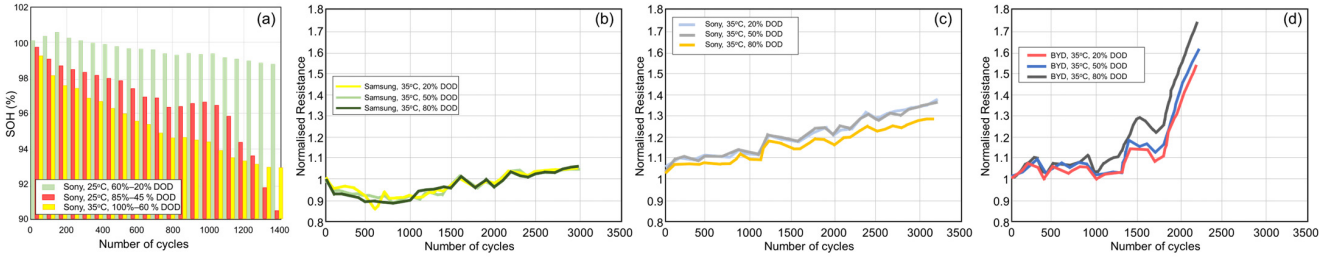


Figure 13. (**a**) SOH variation for different DOD's range; (**b**) resistance increase for Samsung (NMC) cells; (**c**) resistance increase for Sony (LFP) cells; (**d**) resistance increase for BYD cells (LFP). This figure is adapted from [23].

In [23], the metal oxide-based NCA and NMC cells exhibit more pronounced degradation as a function of DOD, compared to LFP cells, which show less sensitivity to depth of discharge. According to the authors [23], this could be explained by the higher operating voltages of NMC and NCA cathodes (up to 4.2 V) compared to LFP cathodes (3.6 V). This difference in battery behavior has already been observed in previous studies.

Sihan Zhang et al. [116], in an experimental study on the SOH estimation of LIBs using EIS, show that a higher DOD leads to greater internal resistances (series resistance R_0, charge transfer resistance R_{ct}) without affecting the degradation rate. This is explained by the more intense electrochemical reactions occurring in the anode at high DOD. As illustrated by Figure 14, a significant increase in R_0 and R_{ct} is observed with the aging of the cells, and higher DODs (100% vs. 80%) result in elevated values of R_0 and R_{ct}, although the rate of increase is not influenced by the DOD.

(f) Influence of SOC

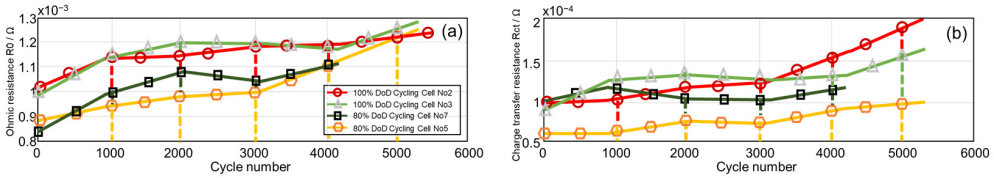


Figure 14. (**a**) Ohmic resistance variations for different values of DOD; (**b**) Charge transfer resistance variations for different values of DOD [116].

Chowdhury et al. [117] aim to understand the dependence of SOC on the aging of NCA/Gr-SiO batteries in a recent mainstream EV, the Tesla Model 3. 21,700 battery cells were taken from a new vehicle and cycled within narrow SOC windows (10%). The results show that the cycled battery cells at very low (<25%) or very high SOC (>90%) degrade more rapidly than those cycled at moderate SOC. The most significant aging was observed for the cells cycled between 5 and 15% SOC, attributed to accelerated loss of the lithium inventory and active material. However, calendar aging is not accelerated by low SOC storage.

Huaiyu Zhong et al. [118], in an experimental study on the thermal behavior and failure mechanisms of 18,650 LIB, raise several points. The study shows that operating LIBs at high states of charge (beyond 100%) leads to faster degradation of their performance. Specifically, the battery's voltage and the internal resistance increase rapidly during overcharging, due to excessive migration of the lithium-ions from the cathode to the anode. This increase in the impedance is accelerated with the number of charge–discharge cycles and results in a significant drop in capacity retention for the most overcharged batteries (108% and 116% SOC), as illustrated in Figure 15a.

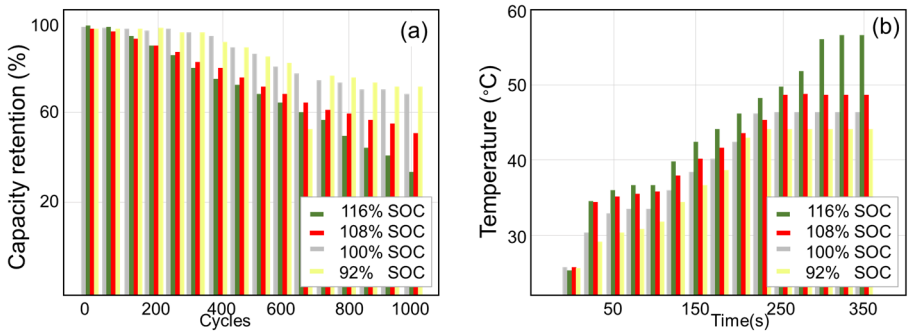


Figure 15. (**a**) Influence of the SOC on capacity retention; (**b**) Influence of the SOC on temperature [118].

Impedance spectroscopy analysis confirms that the charge transfer resistance increases with SOC, linked to electrolyte decomposition, collector corrosion, and SEI formation. These detrimental effects of overcharging also manifest as reduced thermal stability. Indeed, under adiabatic conditions, the surface temperature of a LIB at 116% SOC is approximately 10 °C higher than that of the battery with 100% SOC (Figure 15b). A higher SOC results in greater energy and power storage within the LIB, making TR reactions more easily triggered.

Furthermore, based on an experimental study, Brand et al. [93] show that the series resistance of an IHR18650A LIB increases with decreasing SOC, which is an exception compared to other LIBs. As the SOC decreases, the semicircle in the Nyquist plot (frequency response of the electrochemical impedance) steadily enlarges, primarily due to the rising impedances of the cathode at low SOC. This indicates an increase in charge transfer resistance R_{ct} at lower SOC levels. Additionally, the corner frequency of the semicircle also changes with SOC. For new batteries, it increases nearly linearly from 155 Hz at 10% SOC to 304 Hz at 70% SOC, while for used batteries at 80% health, it changes from 86 Hz at 10% SOC to 181 Hz at 70% SOC. This partially linear trend can be attributed to the increase in R_{ct} at low SOC, within the RC model framework. In summary, the LIB's impedance varies significantly based on SOC in an atypical manner compared to other battery technologies.

At high SOC, electrochemical reactions produce more heat, which can lead to more intense combustion, promoting increased oxygen consumption and thus more significant exothermic reactions. This is supported by the work performed by Peng et al. [119], who also evaluate and analyze the toxic risk of the 68Ah LFP battery. The main gasses emitted include hydrogen fluoride and sulfur dioxide, both of which have particularly severe effects, and their production increases with the higher SOC.

In the same vein, Bugryniec et al.'s [44] synthetic work highlights the impact of the SOC on gas production during TR. Generally, an increase in SOC is associated with a greater generation of specific volumes of emitted gas, particularly for NMC and LCO chemistries. At high SOC, NMC cells produce more CO_2, while LFP cells primarily emit electrolyte vapors. The toxicity of the emitted gasses also varies with SOC. For NMC, the contaminated volume doubles from 0% to 100% of SOC, whereas for LFP, it decreases by half. The composition of the gasses, which mainly include CO_2, CO, H_2, and hydrocarbons, changes according to the SOC and the chemistry of the battery's cell.

The effects of optimal SOC windows are analyzed by Wikner et al. [120]. The capacity of the cell is defined by a voltage range, where 2.8 V corresponds to 0% SOC and 4.15 V to 100% SOC, according to the manufacturer. The cells use an organic electrolyte of 1 M LiPF6, a natural graphite anode, and a cathode made of a mix of LMO and NMC. Key observations are summarized in Table 5, noting that lower SOC ranges enhance battery durability.

Table 5. Analysis of SOC effects on battery durability.

SOC	C-Rate	Remarks
0–10%	+2 C/−2 C	Cells tested at the three lowest SOC levels (0–10%, 10–20%, and 20–30%) exceed expectations in cycle duration, retaining capacity slowly over time. In contrast, cells in larger SOC ranges (0–90%, 80–90%, and 10–90%) reach their cycle limit (below 3200 full cycle equivalents (FCEs)) more quickly under the same conditions (25 °C, 35 °C, and 45 °C).
10–20%	+1 C/−1 C +2 C/−2 C +4 C/−4 C	
20–30%	+2 C/−2 C	
30–40%	+2 C/−2 C	Robust capacity retention, a slight increase in resistance.
40 to 50%	+2 C/−2 C	For the 40 to 50% SOC range tested at +2 C/−2 C, degradation differences between the three temperatures (25 °C, 35 °C and 45 °C) were negligible.
60–70%	+1 C/−1 C +2 C/−2 C +4 C/−4 C	- Cells tested at higher SOC levels (60–70%, 70–80%, and 80–90%) show similar initial capacity retention to those in larger SOC ranges (0–90%, 80–90%, and 10–90%), but they degrade more slowly after 2000 FCE; - The smallest increase in resistance is observed for the cells tested at 80 to 90% SOC at 25 °C.
70–80%	+2 C/−2 C	
80–90%	+1 C/−2 C +2 C/−2 C	
10 to 90%	+1 C/−2 C	- Faster aging at 45 °C (the cell with a +1 C charge rate ages faster in FCE than the one with a +2 C rate); - The cells in the SOC range of 10 to 90% with a +1 C charge and −2 C discharge rate have an average of 7.2 FCE per day; - At 25 °C, the cells show similar capacity retention, indicating that temperature significantly affects aging and performance.
0 to 90%	+1 C/−2 C +2 C/−2 C	- The cells in the SOC range of 0 to 90% with a +2 C charge and −2 C discharge rate have a rate of 9.5 FCE per day; - The cells tested in the SOC ranges of 0 to 90% and 10 to 90% show a greater increase in resistance compared to the cells tested at 80 to 90% SOC.

The study also provides insights into degradation mechanisms, specifically lithium loss inventory (LLI) and loss active material ($LAM_{cathode}$ and LAM_{anode}). The analysis is based on variations in open-circuit voltage (OCV), as described by Equation (4):

$$V_{cell} = V_{cathode} - V_{anode} \quad (4)$$

where the electrode voltage is connected to the degree of lithiation of the material. As the cell ages, changes in OCV are observed.

The impact of SOC on LAM_{anode} and $LAM_{cathode}$ (Figure 16, [120]) is reflected in an increase in active material loss in the PE at higher SOC levels, particularly evident for cells tested at 25 °C. Cells operating at 60–70% SOC exhibit a more significant $LAM_{cathode}$, indicating a rise in secondary reactions. Similarly, LAM_{anode} is generally higher at elevated SOC, suggesting that these conditions lead to greater losses. At lower SOC levels (0–10%), a decrease in LAM_{anode} is observed with increasing temperature, contrasting with the behavior at higher SOC. Regarding LLI, it also increases with higher SOC, especially at 80–90% SOC, where secondary reactions consuming lithium are favored. In summary, high SOC results in increased active material loss, a rise in secondary reactions, and an elevation in LLI.

(g) SOC and Calendar Aging

As indicated in Figure 6, SOC is closely related to calendar aging. Numerous studies establish a correlation between SOC and calendar aging [121,122], indicating that capacity loss increases with SOC. However, the work of Keil et al. [123] reveals a nonlinear degradation over time, depending on the value of the SOC. These investigations focus on LFP (1.1 Ah/2.0 V–3.6 V/Graphite Anode), NMC (2.05 Ah/2.75 V–4.2 V/Graphite Anode), and NCA (2.8 Ah/2.5 V–4.2 V/Graphite Anode) technologies.

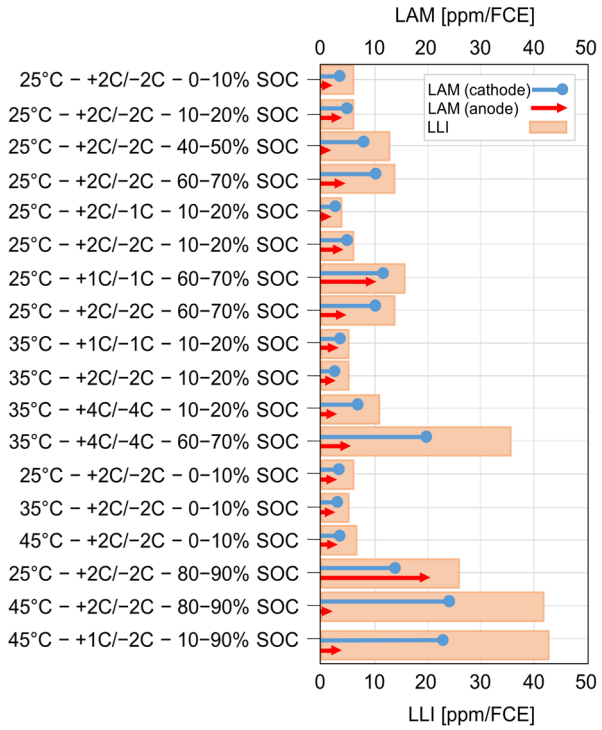


Figure 16. Estimated LAM and LLI per FCE for 15 of the tested cells [120].

The results show significant plateaus around 60% of SOC for NCA and NMC cells, and above 70% for LFP cells. Furthermore, NMC cells exhibit increased capacity loss at SOC levels above 70%. The resistance increase is the lowest for LFP cells, which do not vary much with SOC. In contrast, for NCA and NMC cells, the resistance increases consistently with SOC, without a direct correlation to the capacity loss. Figure 17a–f presents six LIB chemistries (NCA, NMC, LFP, LCO, LMO, and LTO-LCO) subjected to three SOC settings (2%, 38%, and 100%) and three ambient temperature conditions (18.5 °C, 50 °C, and 60 °C). Geisbauer et al. [124] illustrate capacity degradation over 120 days. The results show that different LIB chemistries degrade differently due to calendar aging with less pronounced degradation for LMO technologies followed by LFP. The extreme conditions, such as a SOC of 100% and high temperatures (like 60 °C), lead to an increase the capacity degradation in the majority of the cases. Overall, the effects of calendar aging are more pronounced at 60 °C than that of 50 °C as illustrated in Figure 17g–i.

(h) Influence of the temperature

The nonlinear characteristics of the LIBs are strongly influenced by the external and internal temperatures of the LIB cell. A cell temperature beyond the safe operating limit specified by the manufacturer affects the degradation of LIBs and can also lead to TR and even fire hazards. Therefore, accurate information about the internal and surface temperature of the cell is crucial for effective thermal management and proper operation of the BMS. While optimal ranges of −30 °C to 55 °C or −20 °C to 60 °C [125] have been identified, LIBs can still operate beyond these limits due to their internal characteristics.

Temperature has a significant impact on the Li-ion battery's performance degradation regardless of the type of electrode material [126,127]. This section provides a brief overview of the main issues that require thermal management of the LIBs. These include capacity and power loss, and thermal runaway, among others.

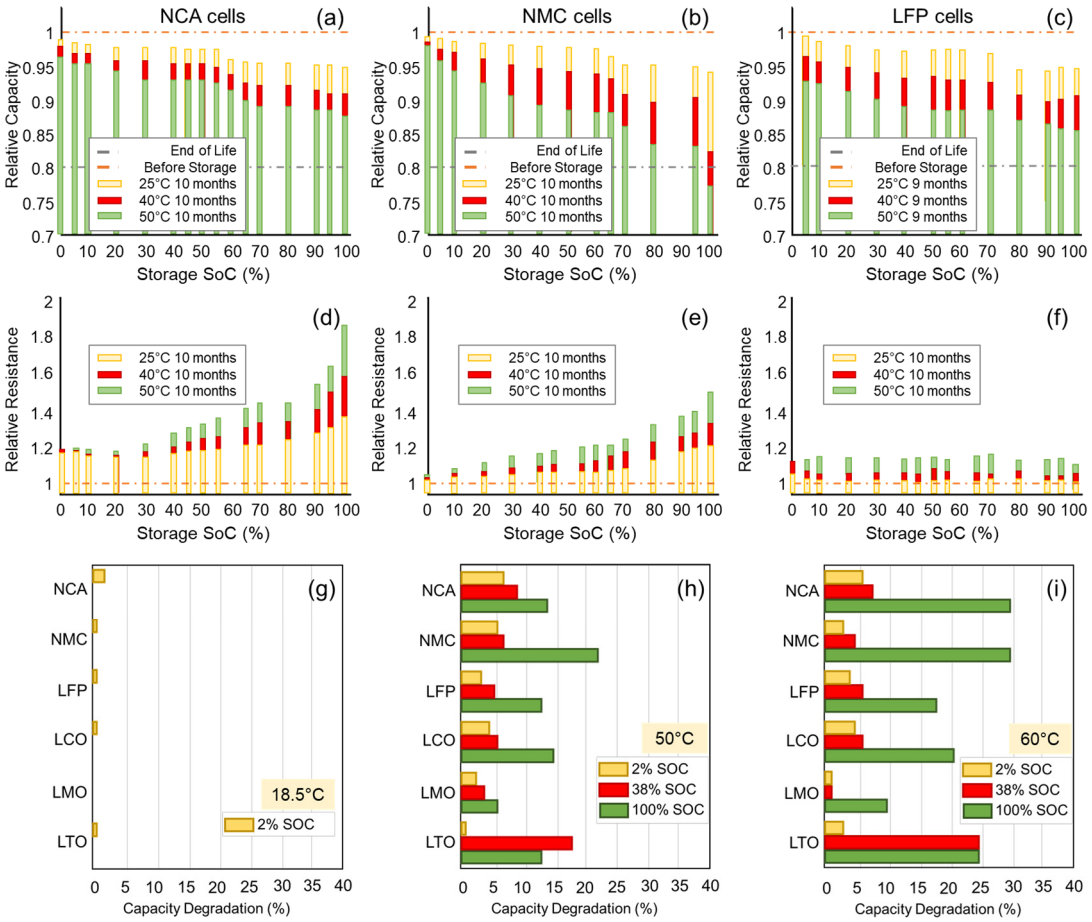


Figure 17. Effect of SOC on relative capacity (**a**–**c**) and relative resistance (**d**–**f**) with different temperature for different cell chemistry; Effect of SOC on capacity with constant temperature for different cell chemistry: (**g**) 18.5 °C, (**h**) 50 °C, (**i**) 60 °C [121–124].

- Low temperature

Numerous studies have established the effects of both low and high temperatures on LIBs. Lowering the temperature leads to a significant drop in the power and energy densities of the LIBs. This phenomenon can be explained by several interdependent mechanisms. First, the increase in electrolyte viscosity at low temperatures reduces ionic conductivity and the transport of the lithium ions through the electrolyte and the SEI layer [128,129]. This results in increased polarization and growth of lithium dendrites [130,131].

Although the drop in the temperature causes similar effects across different types of LIBs, electrolytes and SEI rich in inorganic species, such as LiF, are found to be more tolerant of temperature changes and more beneficial for Li^+ ion transport [132]. The study conducted on the LFP batteries by Manh-Kien Tran et al. in [133] shows that equivalent circuit model (ECM) parameters (ohmic resistance R_0, which includes electronic and ionic resistance of current collectors, electrodes, active material, electrolyte, and separator, and polarization resistance R_1) were strongly dependent on the SOH, SOC, and temperature. Indeed, R_0 increased with decreasing the temperature and SOH, while R_1 rose at low temperatures.

Experimental work performed by Dongxu Ouyang et al. [134] confirms this approach, where experimental results from an NMC 532/graphite cell (1300 mAh; [4.2 V, 2.75 V]) show that the battery experiences a more significant temperature increase when the ambient temperature is low. This is explained by the fact that the internal resistance of the battery is high at low temperatures, resulting in greater heat generation within the battery. Furthermore, this study draws a parallel between capacity changes at ambient temperature

(25 °C) and low temperature (0 °C). At ambient temperature, capacity initially increases and then fluctuates around a stabilized value, with better performance at low cycling rates. In contrast, at low temperatures, capacity gradually decreases, with a more rapid decline at high cycling rates, indicating accelerated aging. Electron microscopy analysis shows that this phenomenon is related to the excessive formation of a passivation layer (SEI) on the anode, which increases impedance, and damages the separator, impairing the transport of active species.

The work of Lecompte et al. [135] examines the impact of fast charging at low temperatures (−20 °C, −10 °C, and 0 °C) on the lifespan of 36 cylindrical NMC cells in the 21,700 format with high nickel content. A rigorous protocol was established, including conditioning cycles, SOH checks, and cyclic aging defined by two protocols: P1 and P2 (Figure 18). The results show that the lifespan of the batteries is significantly reduced at low temperatures, even under nominal charge currents. The P1 protocol stops discharge at a voltage of 3.65 V, while the P2 protocol involves a systematic discharge of 50% of the nominal capacity Q_0. It was observed that P2 degrades the cells more rapidly than P1 under equivalent current and temperature conditions, due to a higher DOD. This situation leads to an increase in the amount of lithium deposited at each recharge when the charge rate allows for it. Significant swelling was observed in several cells, particularly those tested under the following conditions: 0 °C/2 C (after approximately 800 cycles at a SOH of about 54%) for P1, and −20 °C/0.3 C (after a few dozen cycles) for P2. Other cells cycled under similar conditions reached an SOH of 46% without failure, indicating a high dispersion of performance at low temperatures.

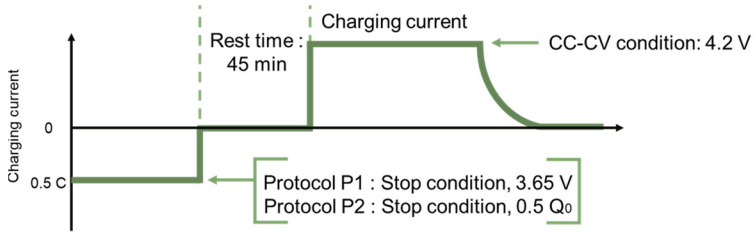


Figure 18. Micro-cycle used in the aging protocols cycling tests [135].

In general, low temperatures primarily result in capacity loss and power loss. They can also precede failures such as ISC. Indeed, the incomplete decomposition of the electrolyte at low temperatures promotes the deposition of metallic lithium in the form of dendrites on the surface of the anode [136]. These dendrites can penetrate the separator and can be modeled as a parallel leakage resistance in the impedance circuit. The electrochemical phenomena and the corresponding equivalent circuits are summarized in Figure 19 [137].

(a) The Hard-Short Circuit arises from the rapid penetration of dendrites and is irreversible. It causes a sudden drop in the voltage [138]. Its unpredictable nature is particularly evident in rigid inorganic solid electrolytes [139];
(b) The Partial Short Circuit represents the initial stage of a complete SC, where the lithium filaments only penetrate the interfaces. It results in a slight voltage drop, indicating a partial reduction in the impedance of the electrolyte volume. The residual impedance characterizes this type of SC as degradation rather than a complete failure;
(c) The Soft Short Circuit is characterized by a slight voltage drop and fluctuations in charge curves, leading to severe overcharging. However, it can often be recovered after regulating external factors [140]. It typically occurs in polymer or hybrid electrolytes.

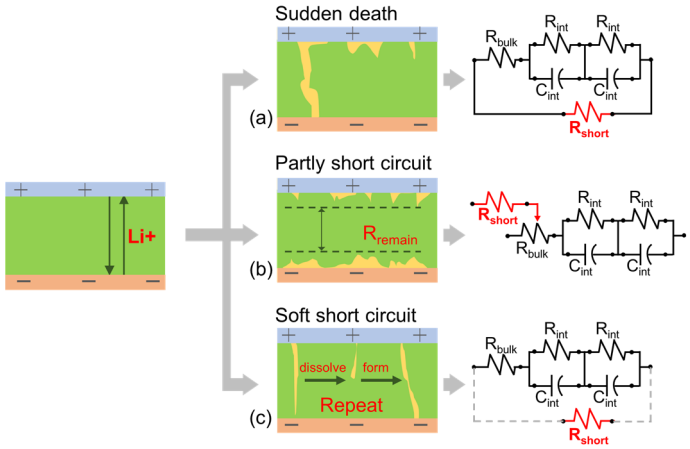


Figure 19. (**a**) Hard short circuit and its ECM; (**b**) Partial short circuit and its ECM; (**c**) Soft short circuit and its ECM.

It is important to note that these types of failures are not exclusively caused by low temperatures. In LIBs, especially those with solid electrolytes, SC is also frequently due to mechanical shocks or unfavorable conditions such as high current density or the presence of impurities, which can promote uneven lithium growth, leading to dendrite formation [137].

- High temperature

Heat generation is inevitable during the charging and discharging phases and is represented by Equation (5).

$$\dot{Q} = I(V-U) + IT\frac{\partial U}{\partial T} - \sum_t \Delta H_t^{avg} r_t - \int \sum_f (\overline{H}_f - \overline{H}_f^{avg}) \frac{\partial C}{\partial t} dv \quad (5)$$

The term $I(V-U)$ represents the irreversible heat generated due to the internal resistance of the LIB and associated circuits. The term $IT\frac{\partial U}{\partial T}$ is the reversible entropic heat. The last term represents the mixing heat, which refers to the heat released or absorbed when different materials mix in a LIB. While Equation (5) clearly shows the relationship between cyclic aging and temperature, the latter also impacts calendar aging, as highlighted by the work of Werner et al. [141] and Ali et al. [142].

While an increase in temperature compared to low temperatures can improve conductivity, it becomes problematic as it approaches 60 °C. One of the first phenomena that may occur is a rapid loss of the SEI at the anode, leading to a loss of capacity [143,144]. However, beyond optimal limits, the batteries face significant risks related to high-temperature operation and potential SC, which can lead to exothermic reactions, separator melting, and TR. This can result in fire or explosion of the battery, as unfortunately occurred with the Boeing 787 Dreamliner. Additionally, the confinement of hundreds of the LIBs in series and parallel to power EVs poses challenges for dissipating the generated heat [145]. This is a significant challenge for manufacturers like Tesla, which have experienced battery fire incidents.

Ohneseit et al. [146] conducted an experimental study comparing the TR behavior of 21,700 LIBs with different cathode materials (NMC, NCA, LFP). The results show that NMC cells react first, but NCA cells enter TR slightly earlier. LFP cells react more slowly and at high temperatures, making them safer; at low SOC (0% and 30%), LFP cells do not enter TR until reaching 350 °C. The study provides valuable experimental data for the design and the simulations of safety in LIB systems. Table 6 provides various details on the composition and performance of the different LIB technologies used.

Table 6. Materials composition and structure.

Parameters	NMC	NCA-IL I	NCA-HE II	NCA-HP	LFP
Separator	PE	PE	PE	PE	PE
Anode chemistry	carbon + 1.6% silicon	carbon + 1.4% silicon	carbon + 1.4% silicon	carbon + 1% silicon	carbon no silicon
Mean capacity (Ah)	4959	4893	4873	3892	3117

The analysis revealed that the disparities in behavior under thermal abuse were primarily attributable to cathode chemistry, rather than other components of the cell such as the electrolyte, anode, or separator, which were similar across the different types of tested cells. This observation highlights the crucial role played by the cathode material in the intrinsic safety of LIBs. A similar conjecture is noted in the findings of Brand et al. [147], where LFP cells exhibit much lower maximum heating rates (7–28 °C/min) compared to NMC and NCA cells (>400 °C/min). The results demonstrate significantly superior thermal stability of the LFP cells, with no exothermic gas emissions. The stability of NMC cells is also greater than that of NCA cells. The technical specifications of the LIBs used are provided in Table 7.

Table 7. Electrical characteristics of investigated cells.

Cathode Chemistry	NMC	NCA	LFP	LFP
Anode chemistry	graphite	graphite	graphite	graphite
Internal Ohmic Resistance (mΩ)	12	24	11	17
Nominal capacity (Ah)	1.5	1.5	1.05	1.1

A significant increase to 100 °C can lead to the degradation of solvents, resulting in gas production, with pressure rising with the temperature until the cell is likely to burst [143]. While ISC is generally caused at low temperatures by dendrite proliferation, it is the melting of the separator that can be one of the causes of such failures at high temperatures (around 135 °C).

The study presented in [148] focuses on four sets of the LIBs that were aged at temperatures of 25 °C, 40 °C, 60 °C, and 80 °C for 100 cycles. The examination of the morphology and composition of the electrodes and separators highlights variations in electric performances and thermal stability. The decomposition products of the SEI layer play a crucial role in the TR behavior. At 60 °C, the accumulation of these products leads to thicker SEI layers and shorter TR times. At 80 °C, these products transform into loosely structured particles, generating a large amount of gas, which results in the rupture of the aluminum-plastic film and the evaporation of the electrolyte, prolonging the duration of TR while decreasing the maximum temperature as illustrated in Figure 20.

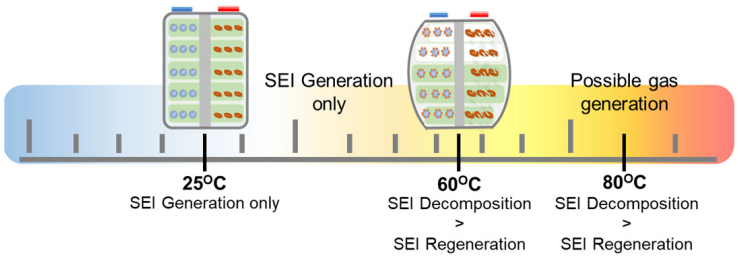


Figure 20. Impact of heat increasing in LIB. This figure is adapted from [148].

Long-term capacity retention tests on a $Li_4Ti_5O_{12}$ (LTO) battery show that, the temperature has a significant impact on the degradation of the battery's performance. Figure 21

indicates that the battery retains 80% of its initial capacity after more than 20,000 cycles at 25 °C, but only 15,000 cycles at 35 °C and 8000 cycles at 45 °C [149]. Thus, increasing the operating temperature significantly accelerates long-term capacity loss, which is a crucial factor for applications requiring high durability.

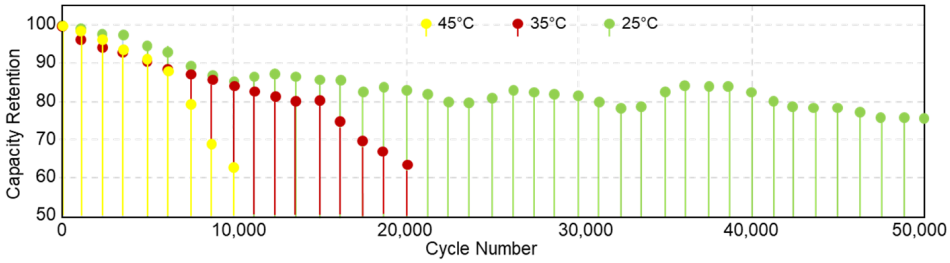


Figure 21. Impact of the temperature on capacity retention [149].

The correlation between the increase in temperature and power capacity was established by Shuping Wang et al. The authors in [55] confirm the impact of the high temperatures on the performance of the LIBs, specifically an NMC-type LIB. The authors measure the internal resistance using hybrid pulse power characteristic (HPPC) tests at different ambient temperatures. Figure 22 illustrates the impact of temperature and to a lesser extent, SOC on the power fade of LIBs.

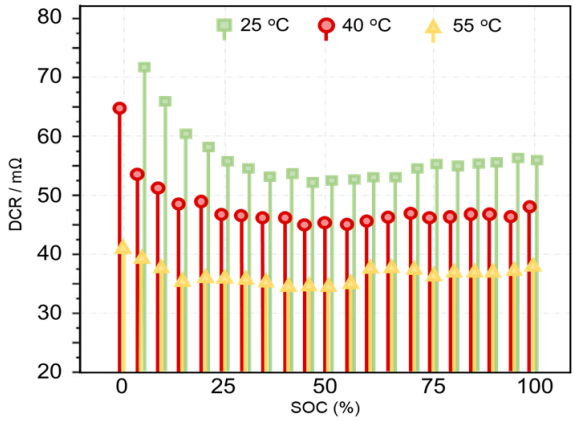


Figure 22. Impact of the temperature on resistance increasing [55].

Another study conducted by Tianfeng Gao et al. [148] analyzed the impact of aging at different temperatures (25 °C, 40 °C, 60 °C, 80 °C) on the thermal stability of NMC batteries cycled in CC-CV. The results indicate that changes in the decomposition products of the passivation layer (SEI) are a key factor. At 60 °C, the accumulation of SEI products thickens the layer and shortens the time to TR. At 80 °C, the SEI products transform into porous particles that generate more gas, leading to casing rupture but prolonging the TR time at a lower maximum temperature. Thus, the high-temperature aging results in significant changes to electric performance and thermal stability, linked to alterations in the SEI layer.

The study conducted by Gailani et al. [53] emphasizes the importance of material types and their characteristics in battery degradation. The study presents experimental data on the degradation of LIBs from three manufacturers: Sony (capacity: 3.0 Ah, nominal voltage: 3.2 V), BYD (capacity: 25 Ah, nominal voltage: 3.2 V) with LFP chemistry, and Samsung (capacity: 94 Ah, nominal voltage: 2.7 V) with NMC chemistry. The NMC cell reached 80% of SOH after 3000 cycles at 35 °C with a DOD of 75%, suggesting a better cycling lifespan compared to the two LFP cells under the same conditions. Moreover, the capacity loss for the Sony cell is 0.33% at 10 °C, 1.33% at 20 °C, and 5.33% at 35 °C. For the

BYD cell, the capacity loss is 6% at 10 °C, 6.4% at 20 °C, and 10% at 35 °C. Although both batteries utilize the same technology and have relatively close voltage ranges, they exhibit different degradation rates. This difference can be attributed to the fact that the BYD LFP battery has a significantly larger nominal capacity, which may depend on factors such as energy density, electrode size, and chemistry, which in this case is the same.

Similarly, to the study on current profiles, Yunhong Che et al. [91] demonstrate that the battery aging is accelerated when exposed to variable temperatures (VT) (25 °C–35 °C–25 °C–15 °C) rather than being maintained at a constant temperature (CT) (25 °C), despite having the same average temperature. Furthermore, the loss of the power occurs more slowly than the loss of the capacity. This indicates that under high currents and variable temperatures, more electrochemical reactions associated with aging take place, in addition to the increase in internal resistance as presented in Figure 23 [95]. This observation highlights the necessity for optimal temperature distribution management in batteries.

(i) Humidity effect

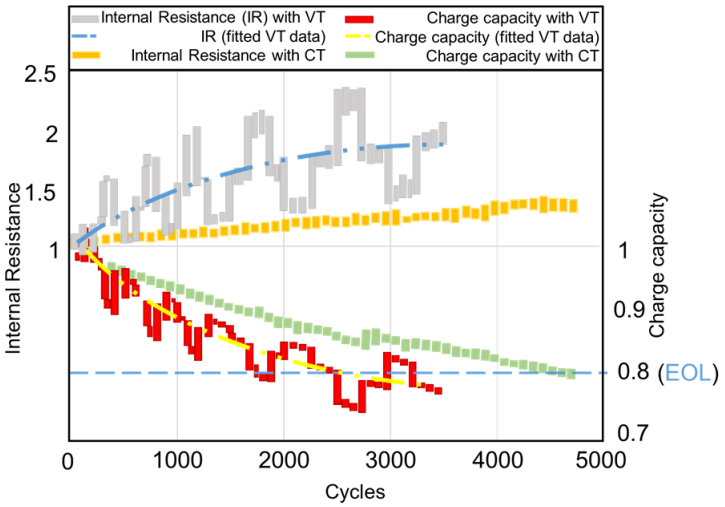


Figure 23. Impact of the temperature profile on internal resistance. This figure is adapted from [91].

Humidity refers to the amount of water vapor present in the air. It plays a crucial role in many natural phenomena and influences health, climate, and materials. Through processes such as moisture formation and corrosion, humidity can also impact the performance, durability, and safety of LIBs.

In their study, Han et al. [150] employed various methods, including scanning electron microscopy (SEM), energy-dispersive X-ray spectroscopy (EDX), and electrochemical impedance spectroscopy (EIS), to analyze batteries based on NMC, graphite, exhibiting both normal and abnormal direct current resistances (DCR). Their research highlights the reasons for the rapid increase in DCR observed in certain batches of LIBs stored at 60 °C, emphasizing the negative impact of excessive humidity during battery production, which leads to degradation of the SEI and CEI. Batteries whose failure is attributed to environmental conditions are referred to as failure batteries (FBs), while those exhibiting normal DCR during high-temperature storage tests are designated as normal batteries (NBs). Table 8 provides a comparative summary between NB and FB batteries.

Moisture content has a significant impact on the increase in DCR and impedance, which affects electrochemical performance. Batteries with controlled humidity levels demonstrate better performance in terms of DCR compared to those with high humidity levels.

Table 8. Comparative summary between NB and FB batteries.

LIBs Parts Chemistry	Details
Anode	- SEM Analysis: similar morphologies; the laminar structure is intact for NB and FB (no cracks or spalling); - EDX Analysis: high levels of oxygen (O) and fluorine (F) detected in the SEI of the FB anode; this suggests that an increase in the thickness of the SEI could lead to abnormal changes in the internal resistance of LIBs; - FB anode contains significantly more lithium than NB anode. This implies that the SEI layer is thicker, as the detected lithium is part of this layer.
Electrolyte (LiPF6)	FB consumes more electrolytes to form SEI/CEI films.
Separators	SEM Analysis: images do not reveal significant differences between the NB and FB groups in the morphology of the separators, both of which maintain good permeability.
Cathode (NCM)	- SEM Analysis: the similarity of the structures of the cathodes in both NB and FB samples suggests that their fabrication was consistent and free of visible defects; - EDX Analysis: no differences in the elemental contents of Ni, Co, or Mn in the active material; - The levels of fluorine (F) and phosphorus (P) in the cathode of the failing LIBs are slightly higher, indicating a change in the composition of the CEI films. The continued growth of the CEI induces an increase in the DCR.

This trend is confirmed by the study by Byun et al. [151], which examines the impact of humidity on the performance of pouch cells, focusing on the differences between treated and untreated LIBs. By using a laminated aluminum film as a barrier against humidity, the researchers demonstrated that treated LIBs, with battery tabs protected by polyimide tape, maintained higher discharge capacity and lower interfacial resistance after storage in humid conditions. The study also distinguishes capacity losses into two categories: reversible and irreversible. Treated LIBs show better retention of reversible capacity, while untreated LIBs experience a greater irreversible capacity loss, especially those based on NCM active material, which exhibit severe degradation compared to LCO-based LIBs. The latter shows much lower discharge capacity loss, even under humid conditions. These results highlight the importance of humidity protection to minimize performance degradation and open avenues for optimizing battery design in challenging environments.

Similar studies, such as that by Zhang et al. [152], provide a detailed analysis of the degradation of the nickel-rich cathode material $LiNi_{0.85}Co_{0.1}Mn_{0.05}O_2$ in a humid environment (63% humidity) over one year, focusing on the physicochemical changes and electrochemical performance. The study highlights the formation of an amorphous layer on the surface of the particles, which alters their morphology and impacts their charge capacity and coulombic efficiency, with a correlation observed between O_2 and CO_2 gas emissions and the state of charge. It also reveals processes of carbonate decomposition and humidity-induced structural degradation, employing techniques such as the X-ray imaging Method and Transmission Electron Microscopy (TEM).

On the other hand, the study of Fullerton-Shirey et al. [153] enhances the understanding of solid polymer electrolytes (SPE) filled with nanoparticles. The study deepens the understanding of SPE filled with nanoparticles by highlighting the significant impact of humidity on crystallization and conductivity. At low humidity, SPEs with an oxygen ether to lithium ratio of 8:1 require 3 days to crystallize, while at high humidity, this process is delayed to 3 weeks. The addition of nanoparticles improves conductivity under specific conditions; at low humidity, their effect is slightly negative, but at high humidity, it becomes positive, especially at a ratio of 10:1. Furthermore, nanoparticles appear to inhibit water absorption in the presence of lithium, although, at the eutectic concentration of 10:1, the samples absorb more water than those at 8:1, suggesting a segregation of nanoparticles in lithium-poor regions. These results underscore the importance of interactions between water, nanoparticles, and lithium ions in optimizing SPE performance, while indicating the need for further research to explore these underlying mechanisms and improve formula-

tions for more effective energy storage technologies by highlighting the significant impact of humidity on crystallization and conductivity.

(j) Mechanical Stress

Mechanical stress or mechanical abuse of the LIBs refers to the damage caused by physical constraints or inappropriate usage conditions. The main causes of mechanical stress include the following: "physical shocks" (impacts, drops, or accidents causing internal damage) and "compression" (excessive pressure deforming the cells).

Ohneseit et al. [146] tested 41 cells distributed across three chemistries (LFP, NMC, and NCA) using nail penetration at four SOC (0%, 30%, 50%, and 100%). No TR occurred at SOC 0%; in contrast, it happened at SOC 30%, 50%, and 100% for the NMC and NCA chemistries, demonstrating greater safety of LFP cells against mechanical abuse.

Zhou et al. [154] examined the dynamic failure of the lithium-ion pouch cells compared to quasi-static tests. The inertia effect of the multilayer structure leads to premature failure under dynamic loading, with a failure threshold lower than that observed in quasi-static conditions. The cells exhibit delayed failure behavior, related to separator degradation or direct contact between electrodes. Irreversible failures can occur without visible signs, making the inflection points of the force/voltage curves unreliable.

Using indentation experiments (ball intrusion, cylindrical intrusion, and out-of-plane compression), Wang et al. [155] explores the failure behaviors and mechanisms of LIBs, focusing on LFP, NMC, and LTO cells under mechanical abuse. The LFP cells exhibit a maximum force of about 21,506 N, a temperature of about 124 °C, and a voltage drop of 3 V. In contrast, the LTO cells increase their force without a significant drop in voltage, experiencing a brittle fracture with a slow decrease in voltage. During ball intrusion tests, both NMC and LFP drop to 0 N, while the LTO gradually decreases to about 10 kN, with no cell failing at 100 kN in out-of-plane compression. Temperatures remain stable during this compression, with high peaks for NMC and LFP at increased SOC, while the LTO shows a gradual increase related to a minor ISC. Finally, ball intrusion causes an ISC in all cells, with SOC influencing the duration of this ISC, while the LFP resists better under cylindrical intrusion and does not trigger an ISC during out-of-plane compression.

Parallel research, such as that of An et al. [156], aligns with some of these findings. Indeed, in an experimental study on failure mechanisms during mechanical abuse, the results indicate that the charge capacity and displacement during a short circuit decrease with increasing SOC, which also leads to a faster temperature rise. Beyond 60% of SOC, TR phenomena, such as explosions, can occur. The mass loss rate depends on the SOC and the thickness of the electrodes, but not on their material. SEM analyses show graphite fractures and more intense electrochemical reactions in NMC electrodes compared to LFP.

Luigi Aiello et al. [157] conducted a study to evaluate the performance of a pouch LIB based on variations in temperature, pressure, and discharge rate. The experimentation was carried out at three temperatures (5 °C, 25 °C, 45 °C), four pressures (0.2 MPa, 0.5 MPa, 0.8 MPa, 1.2 MPa), and three discharge rates (0.5 C, 1.5 C, 3.0 C).

The results show that electrochemical processes and overall efficiency are significantly influenced by temperature and pressure, thus affecting capacity and charge–discharge rates. In particular, an increase in pressure tends to decrease performance, while a rise in temperature improves it. However, the extent of the pressure's impact on performance varies depending on the temperature and the applied discharge rate. For instance, at 5 °C and a discharge rate of 0.5 C, an increase in pressure from 0.2 MPa to 1.2 MPa results in a reduction of 5.84% in discharged capacity, whereas at 45 °C, this decrease is only 2.17%. A summary scheme of the amount of energy extracted under all the considered conditions is presented in Figure 24.

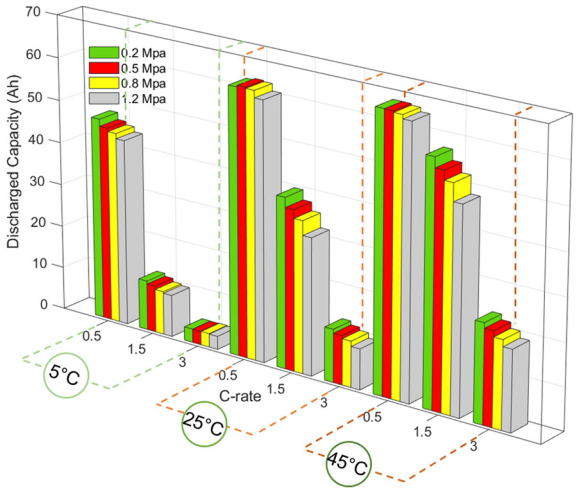


Figure 24. Overview of the extracted charge under different conditions [157].

4. Battery Management System (BMS)

The configuration of cells in a battery pack is tailored to meet the electrical requirements of a system. Series connections provide the desired voltage (Figure 25c), while parallel connections increase the capacity (Figure 25b). For example, multiple low-capacity cells can be connected in parallel to form modules, which are then arranged in series to boost voltage (Figure 25e), as implemented in the Tesla Model S. Alternatively, high-capacity cells can be connected in series (Figure 25c), as demonstrated in the Mitsubishi i-MiEV [158].

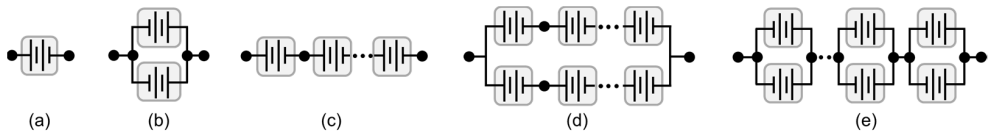


Figure 25. Schematic representations of various battery pack topologies: (**a**) single cell; (**b**) parallel connection; (**c**) series connection of *n* cells; (**d**) parallel connection of two strings; (**e**) series connection of *n* modules, each containing two cells in parallel [158].

To ensure effective management of the various battery configurations forming a pack, it is essential to use a BMS. The BMS is an essential electronic device that monitors, manages, and protects a battery or battery pack. Its absence or malfunction can lead to electrical failures and accelerate degradation mechanisms. The complexity of its configuration depends on the application being investigated. There are three main implementation topologies available in the BMS market: centralized, modular, and decentralized; Like illustrates by Figure 26.

(a) In a centralized BMS, a single unit controls all the battery cells in series. This configuration is cost-effective and easy to maintain, but it poses risks of short circuits and limits scalability due to complex wiring. It is generally suited for batteries with a small number of cells, with a few exceptions like the BMS in the Nissan Leaf [159,160];

(b) Modular BMS connects the cells through multiple identical circuit boards linked to a main control board. The master–slave configuration enhances performance and reduces costs by delegating certain functions to the slave boards, providing a secure and flexible solution for large battery packs [159,160];

(c) In a decentralized BMS, each pack module has its own BMS, operating independently while being interconnected with others. This configuration is common in renewable energy storage systems, where the modules communicate with a central

system for data collection. While it offers great flexibility, it is also more complex and expensive [159,160].

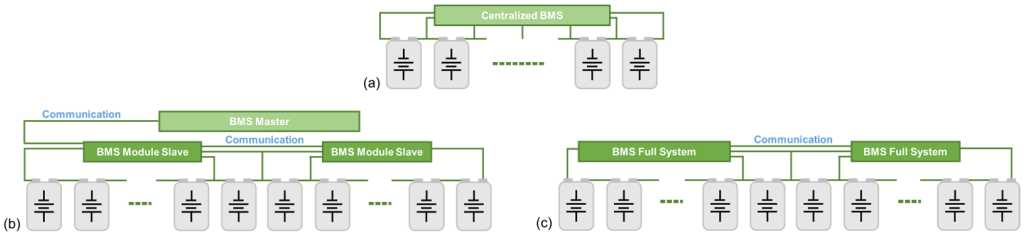


Figure 26. Typical topology of large-scale battery pack BMS systems. (**a**) Centralized network; (**b**) modularized/distributed network; (**c**) decentralized [159].

The effective management of hardware architectures is closely linked to software architecture. This part of BMS incorporates multitasking capabilities. It not only enables the execution of critical functions such as voltage and current measurement, overcurrent and overvoltage protection, and temperature measurement, but can also extend to additional functions depending on the specific applications being investigated, such as cell balancing, fault detection, and diagnostics [161]. It is generally structured in modules, with functional units such as cell monitoring and thermal management (battery thermal management system (BTMS)) interconnected by communication channels.

The acquisition of the temperature of the cells and peripheral components is essential in the design of a BMS. This involves selecting the appropriate sensors and locations to avoid reading errors. To prevent failures of LIB caused by critical temperatures, a well-designed BTMS is essential. It must ensure optimal battery operation by maintaining a uniform temperature distribution. These cooling systems are divided into two main categories, internal BTMS and external BTMS, as shown in Figure 27.

(a) Internal BTMS

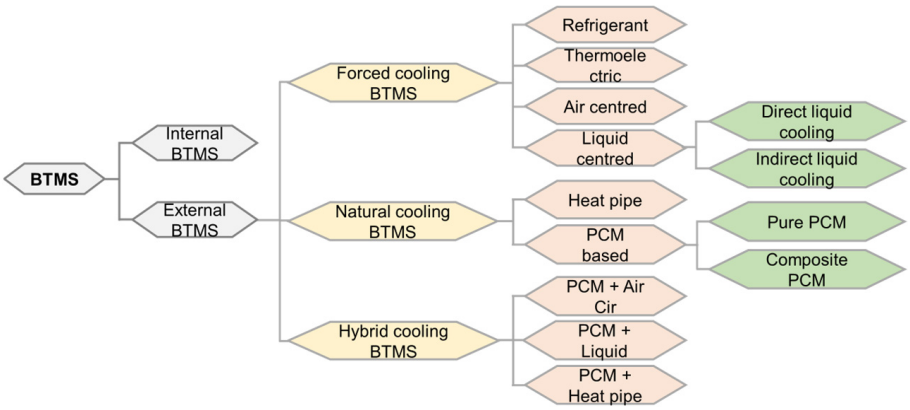


Figure 27. Classification of thermal management systems for batteries. This figure is adapted from [43].

Internal BTMS focuses on optimizing the thermal management of batteries by modifying their internal components. Researchers have suggested various strategies to enhance performance, including cathode coatings, electrode modifications, and axial cooling (Table 9).

(b) External BTMS

Table 9. Overview of internal battery thermal management system approaches.

Approaches	Description	Advantages	Disadvantages
Cathode Coatings [162].	Use of carbon, graphene, and oxides to enhance the electrochemical reaction rate and conductivity of the cathode.	Improve the electrochemical reaction rate and conductivity of the cathode.	Modifications may reduce energy storage capacity, affecting long-term suitability.
Electrode Modifications [163].	Adjusting electrode thickness minimizes internal resistance while balancing energy density and capacity.	Reduce internal resistance, enhancing overall battery performance.	Changes may negatively affect energy density, requiring a balance.
Axial Cooling [164,165].	Creation of a fluidic channel improves cooling efficiency but slightly reduces cell volume.	Offer high cooling efficiency and a low-temperature gradient, enhancing thermal management.	Enlarging the channel for improved cooling may slightly reduce cell volume.

External BTMS differs from Internal BTMS, which modifies battery specifications to enhance cooling, by focusing on external cooling methods without altering the design of the cells. They can be categorized into the following: (i) forced or active systems: extract heat via circulating air or liquid coolants, requiring external power; (ii) natural or passive systems: utilize materials like Phase Change Materials (PCM) to regulate temperature, though PCM's poor thermal conductivity limits effectiveness; (iii) hybrid systems: combine active and passive methods, integrating PCM with liquid or air circulation (Table 10 [42]).

Table 10. Overview of external BTMS approaches [43].

Approaches		Description	Advantages	Disadvantages
Forced or Active	Air-based	Uses natural or forced convection to cool batteries.	Low cost; simple installation; Lightweight; easy maintenance; in direct contact with the battery	Limited efficiency; temperature inequalities; poor performance in high-temperature conditions; additional fan necessary
	Liquid-based	Cooling through conduction and convection using a liquid medium.	High thermal efficiency; better temperature uniformity; suitable for heavy-duty applications; in direct contact with the battery	System complexity; risk of leaks; additional weight
	Based on the thermoelectric	Uses the Peltier effect for cooling.	Simple design; low energy consumption; necessitate no internal chemical reaction; low maintenance cost	Limited efficiency; high material costs; performance affected by extreme temperatures; more electricity required
	BTMS using refrigerants	Utilizes a vapor compression cycle for cooling.	High efficiency; uniform cooling; easy integration.	High cost; system complexity; high energy consumption
Natural or passive	Heat Pipes-based	A thermodynamic system in a vacuum that changes the state of the working fluid (liquid to vapor) to conduct heat.	High thermal conductivity; portability and reliability; low maintenance costs; long lifespan.	Leakage issue; highly intricate structure; significant start-up and continuing expenses

Table 10. *Cont.*

Approaches		Description	Advantages	Disadvantages
	PCM-based	PCMs absorb or release heat during phase transitions (melting and solidification).	Market-available, non-toxic materials; chemical compatibility with traditional construction elements; low price; an even distribution of temperature.	Limited to specific temperature ranges, PCMs may underperform outside these limits, and phase changes can complicate design due to volume changes.
Hybrid		A combination of several cooling methods (air, liquid, PCM, heat pipes) to maintain the optimal temperature of battery packs.	Good thermal distribution throughout the battery pack; excellent natural convection capabilities; additional capability to exhaust heat to the exterior	Exorbitant cost and complexity

In addition to temperature measurement, the design of a BMS may need to address other specific application requirements, such as [165,166]:

- Voltage and current acquisition (for individual cells, stacks, or the entire pack);
- Over-current and over-voltage protection;
- Under-voltage protection;
- Energy management;
- Signal acquisition and filtering;
- Data logging and analysis;
- Data storage;
- Charge and discharge control.

In the context of BMS development and battery aging, it is crucial to consider the relevant technical standards that assess their performance and safety. These standards provide a framework to ensure optimal battery operation throughout their lifecycle. The work of Gabbar et al. [167] offers an in-depth analysis of the technical standards and their impact on battery management for transportation electrification and stationary applications.

Although BMS has advanced, challenges remain in accurately estimating internal parameters, such as SOC and SOH. Limitations in computing power and data storage complicate this task, but recent solutions using the Internet of Things (IoT), twin models, cloud computing, and machine learning aim to overcome these obstacles [168,169].

5. Conclusions

The performance and aging of lithium-ion batteries (LIBs) are governed by complex physicochemical processes influenced by various operating variables. A thorough understanding of the degradation and failure mechanisms of LIBs is essential for optimizing their performance and ensuring their safety. This review has highlighted the significant impact of time, electrical stress, mechanical abuse, temperature, and operating conditions such as state of charge (SOC) and depth of discharge (DOD) on the aging and failure of LIBs.

Although current can induce mechanical stress on active materials, leading to cracks or delamination in the electrodes, its effects are closely linked to temperature. This temperature influence is not limited to the stress caused by electrical current; it also manifests in other causes of LIB degradation, including SOC and DOD. In fact, temperature affects the electrochemical reactions inside the battery, thereby impacting the SOC and DOD. Higher temperatures generally increase the speed of these reactions, which can lead to faster charging and discharging. Moreover, temperature is the parameter most likely to cause failures such as short circuits and thermal runaway. Therefore, enhanced temperature monitoring

could improve the lifespan of LIBs through battery management systems (BMS). Managing temperature is one of the key functionalities of the BMS, which aims to anticipate failures and optimize the useful life of LIBs.

While the influence of all these parameters is relatively well understood, it remains crucial to advance testing practices, which often remain "ideal", typically based on constant current and constant temperature protocols. A more realistic approach to battery stress conditions could lead to a better understanding of their operation, more accurate SOH prediction models, and improved design of BMS. However, it is important to note that some conclusions drawn from these tests may be biased. Indeed, the differences in power levels or capacities often observed highlight the need to establish new comparative benchmarks among different battery technologies. To identify the most effective materials for specific applications, it is essential to conduct tests with batteries that have relatively similar baseline characteristics, cycled under identical conditions, while ensuring significant repeatability. All these issues reveal the importance of making field failure data accessible, thus emphasizing the collaboration between researchers and industry to improve the safety and reliability of batteries. By synthesizing this information, we hope to inform researchers and engineers about the challenges associated with LIBs and guide future research efforts toward strategies for mitigating degradation. However, while an integrated approach that considers testing under ideal conditions has proven effective, incorporating real operating conditions into testing phases could greatly enhance the durability of the LIBs, thereby contributing to a broader and safer adoption of this technology in our modern society.

Author Contributions: The manuscript was written through contributions from J.S.M., M.-B.C. and B.D. All authors have read and agreed to the published version of the manuscript.

Funding: This work is supported by the Normandy region and University of Le Havre Normandie.

Data Availability Statement: Data are contained within the paper.

Acknowledgments: This work is conducted at GREAH Laboratory, University of Le Havre Normandie, particularly by the research team focused on Renewable Energies and Storage Systems (MERS). The authors would like to thank the Normandie Region and the University of Le Havre Normandie for their financial support.

Conflicts of Interest: The authors declare no conflicts of interest.

Abbreviations

AC	Alternating Current
ACP	Alternating Current Pulse
BMS	Battery Management System
BTMS	Battery Thermal Management System
CC	Constant Current
CEI	Cathodic Electrolyte Interphase
CHB	Cascade H-Bridge
CID	Current Interrupt Device
CL	Conductivity Loss
CV	Constant Voltage
CVNP	Constant Voltage Negative Pulse
DC	Direct Current
DCR	Direct Current Resistance
DOD	Depth of Discharge
DVA	Differential Voltage Analysis

EIS	Electrochemical Impedance Spectroscopy
EOL	End of Life
EV	Electric Vehicle
FCE	Full Cycle Equivalent
HF	High Frequency
HPPC	Hybrid Pulse Power Characterization
ICA	Incremental Capacity Analysis
ISC	Internal Short Circuit
LAM	Loss of Active Materials
LIB	Lithium Ion Battery
LLI	Loss of Lithium Inventory
LCO	Lithium Cobalt Oxide
LF	Low Frequency
LFP	Lithium Iron Phosphate
LiF	Lithium Fluoride
LMO	Lithium Manganese Oxide
LMR	Lithium Manganese Rich
LNMO	Lithium Manganese Nickel Oxide manganese nickel oxide
LTO	Lithium Titanate Oxide
MCC	Multi-Stage Constant Current
NCA	Nickel Cobalt Aluminum
NMC	Nickel Manganese Cobalt
NPC	Negative-Pulsed Charging
PAM	Pulse Amplitude Modulation
PCCC	Pulsed Current with Constant Current
PPC	Positive Pulsed Current
PWM	Pulse-Width-Modulation
R_{ct}	Charge transfer resistance
RC	Resistance–Capacitance
SC	Short Circuit
SCC	Sinusoidal half-wave current function
SPCC	Sinusoidal Half-Wave Positive-Pulse Current Charging
SEI	Solid Electrolyte Interphase
SEM	Scanning Electron Microscopy
SOC	State of Charge
SOH	State of Health
SRC	Sinusoidal Ripple Current
TEM	Transmission Electron Microscopy
TR	Thermal Runaway
UDDS	Urban Dynamometer Driving Schedule
WLTC	Worldwide Harmonized Light-Duty Test Cycle

References

1. Xiang, J.; Wei, Y.; Zhong, Y.; Yang, Y.; Cheng, H.; Yuan, L.; Xu, H.; Huang, Y. Building Practical High-Voltage Cathode Materials for Lithium-Ion Batteries. *Adv. Mater.* **2022**, *34*, 2200912. [CrossRef] [PubMed]
2. Ding, Y.; Jiang, Y.; Zeng, C.; Jin, H. Recent progress of advanced separators for Li-ion batteries. *J. Mater. Sci.* **2024**, *59*, 12154–12176. [CrossRef]
3. Maiyalagan, T.; Elumalai, P. *Rechargeable Lithium-Ion Batteries: Trends and Progress in Electric Vehicles*, 1st ed.; CRC Press: Boca Raton, FL, USA, 2021. [CrossRef]
4. Shchurov, N.I.; Dedov, S.I.; Malozyomov, B.V.; Shtang, A.A.; Martyushev, N.V.; Klyuev, R.V.; Andriashin, S.N. Degradation of Lithium-Ion Batteries in an Electric Transport Complex. *Energies* **2021**, *14*, 8072. [CrossRef]
5. Kamaya, N.; Homma, K.; Yamakawa, Y.; Hirayama, M.; Kanno, R.; Yonemura, M.; Kamiyama, T.; Kato, Y.; Hama, S.; Kawamoto, K.; et al. A lithium superionic conductor. *Nat. Mater.* **2011**, *10*, 682–686. [CrossRef]

6. Tatsumisago, M.; Nagao, M.; Hayashi, A. Recent development of sulfide solid electrolytes and interfacial modification for all-solid-state rechargeable lithium batteries. *J. Asian Ceram. Soc.* **2013**, *1*, 17–25. [CrossRef]
7. Minami, T.; Hayashi, A.; Tatsumisago, M. Recent progress of glass and glass-ceramics as solid electrolytes for lithium secondary batteries. *Solid State Ion.* **2006**, *177*, 2715–2720. [CrossRef]
8. Volta Foundation. *The Battery Report 2022*; Volta Foundation: San Francisco, CA, USA, 2023.
9. Wu, F.; Yushin, G. Conversion Cathodes for Rechargeable Lithium and Lithium-Ion Batteries. *Energy Environ. Sci.* **2017**, *10*, 435–459. [CrossRef]
10. Yi, H.; Liang, Y.; Qian, Y.; Feng, Y.; Li, Z.; Zhang, X. Low-Cost Mn-Based Cathode Materials for Lithium-Ion Batteries. *Batteries* **2023**, *9*, 246. [CrossRef]
11. Olbrich, L.F.; Xiao, A.W.; Pasta, M. Conversion-Type Fluoride Cathodes: Current State of the Art. *Curr. Opin. Electrochem.* **2021**, *30*, 100779. [CrossRef]
12. Fu, W.; Wang, Y.; Kong, K.; Kim, D.; Wang, F.; Yushin, G. Materials and Processing of Lithium-Ion Battery Cathodes. *Nanoenergy Adv.* **2023**, *3*, 138–154. [CrossRef]
13. Kainat, S.; Anwer, J.; Hamid, A.; Gull, N.; Khan, S.M. Electrolytes in Lithium-Ion Batteries: Advancements in the Era of Twenties (2020's). *Mater. Chem. Phys.* **2024**, *313*, 128796. [CrossRef]
14. Zhou, L.; Zhang, K.; Hu, Z.; Tao, Z.; Mai, L.; Kang, Y.-M.; Chou, S.-L.; Chen, J. Recent Developments on and Prospects for Electrode Materials with Hierarchical Structures for Lithium-Ion Batteries. *Adv. Energy Mater.* **2017**, *8*, 1701415. [CrossRef]
15. Hossain, H.M.; Chowdhury, M.A.; Hossain, N.; Islam, A.M.; Mobarak, H.M. Advances of lithium-ion batteries anode materials—A review. *Chem. Eng. J. Adv.* **2023**, *16*, 100569. [CrossRef]
16. Li, X.; Yang, Z.; Fu, Y.; Qiao, L.; Li, D.; Yue, H.; He, D. Germanium anode with excellent lithium storage performance in a germanium/lithium–cobalt oxide lithium-ion battery. *ACS Nano* **2015**, *9*, 1858–1867. [CrossRef]
17. Wang, L.; Wang, M.; Jiao, L.; Wang, H.; Yang, J.; Dong, X.; Bi, T.; Ji, S.; Liu, L.; Hu, S.; et al. Pyramid-patterned germanium composite film anode for rechargeable lithium-ion batteries prepared using a one-step physical method. *Coatings* **2023**, *3*, 555. [CrossRef]
18. Baggetto, L.; Notten, P.P.H.L. Lithium-ion (De)insertion reaction of germanium thinfilm electrodes: An electrochemical and in situ XRD study. *J. Electrochem. Soc.* **2009**, *156*, A169–A175. [CrossRef]
19. Manthiram, A. A reflection on lithium-ion battery cathode chemistry. *Nat. Commun.* **2020**, *11*, 1550. [CrossRef]
20. Xue, L.; Ueno, K.; Lee, S.-Y.; Angell, C.A. Enhanced performance of sulfone-based electrolytes at lithium ion battery electrodes, including the $LiNi_{0.5}Mn_{1.5}O_4$ high voltage cathode. *J. Power Sources* **2014**, *262*, 123–128. [CrossRef]
21. Das, D.; Manna, S.; Puravankara, S. Electrolytes, Additives and Binders for NMC Cathodes in Li-Ion Batteries—A Review. *Batteries* **2023**, *9*, 193. [CrossRef]
22. Finegan, D.P. X-Ray Imaging of Failure and Degradation Mechanisms of Lithium-Ion Batteries. Ph.D. Thesis, UCL (University College London), London, UK, 2016.
23. Preger, Y.; Barkholtz, H.M.; Fresquez, A.; Campbell, D.L.; Juba, B.W.; Romàn-Kustas, J.; Ferreira, S.R.; Chalamala, B. Degradation of Commercial Lithium-Ion Cells as a Function of Chemistry and Cycling Conditions. *J. Electrochem. Soc.* **2020**, *167*, 120532. [CrossRef]
24. Faraday Institution. Developments in Lithium-Ion Battery Cathodes. *Faraday Insights* **2023**, *18*, 1–12.
25. Fehse, M.; Etxebarria, N.; Otaegui, L.; Cabello, M.; Martín-Fuentes, S.; Cabañero, M.A.; Monterrubio, I.; Elkjær, C.F.; Fabelo, O.; Enkubari, N.A.; et al. Influence of Transition-Metal Order on the Reaction Mechanism of LNMO Cathode Spinel: An Operando X-ray Absorption Spectroscopy Study. *Chem. Mater.* **2022**, *34*, 6529–6540. [CrossRef] [PubMed]
26. Pieczonka, N.P.W.; Liu, Z.; Lu, P.; Olson, K.L.; Moote, J.; Powell, B.R.; Kim, J.-H. Understanding Transition-Metal Dissolution Behavior in $LiNi_{0.5}Mn_{1.5}O_4$ High-Voltage Spinel for Lithium Ion Batteries. *J. Phys. Chem.* **2013**, *117*, 15947–15957. [CrossRef]
27. Cheng, H.; Shapter, J.G.; Li, Y.; Gao, G. Recent progress of advanced anode materials of lithium-ion batteries. *J. Energy Chem.* **2020**, *57*, 451–468. [CrossRef]
28. Yi, T.-F.; Jiang, L.-J.; Shu, J.; Yue, C.-B.; Zhu, R.-S.; Qiao, H.-B. Recent development and application of $Li_4Ti_5O_{12}$ as anode material of lithium ion battery. *J. Phys. Chem. Solids* **2010**, *71*, 1236–1242. [CrossRef]
29. Li, X.; Ma, W.; Zhang, Y. Electrode Materials for Flexible Lithium-Ion Batteries Based on Carbon Nanomaterials. *Highlights Sci. Eng. Technol.* **2024**, *84*, 73–80. [CrossRef]
30. Feng, K.; Li, M.; Liu, W.; Kashkooli, A.G.; Xiao, X.; Cai, M.; Chen, Z. Silicon-Based Anodes for Lithium-Ion Batteries: From Fundamentals to Practical Applications. *Small* **2018**, *14*, 1702737. [CrossRef] [PubMed]
31. Ding, R.; Huang, Y.; Li, G.; Liao, Q.; Wei, T.; Liu, Y.; Huang, Y.; He, H. Carbon Anode Materials for Rechargeable Alkali Metal Ion Batteries and in-situ Characterization Techniques. *Front. Chem.* **2020**, *8*, 607504. [CrossRef]
32. Yang, J.; Zhou, X.-Y.; Li, J.; Zou, Y.-L.; Tang, J.-J. Study of nano-porous hard carbons as anode materials for lithium ion batteries. *Mater. Chem. Phys.* **2012**, *135*, 445–450. [CrossRef]

33. Chang, H.; Wu, Y.-R.; Han, X.; Yi, T.-F. Recent developments in advanced anode materials for lithium-ion batteries. *Energy Mater.* **2021**, *1*, 100003. [CrossRef]
34. Ullah, K.; Shah, N.; Wadood, R.; Khan, B.M.; Oh, W.C. Recent trends in graphene-based transition metal oxides as anode materials for rechargeable lithium-ion batteries. *Nano Trends* **2023**, *1*, 100004. [CrossRef]
35. Fujimoto, H.; Tokumitsu, K.; Mabuchi, A.; Chinnasamy, N.; Kasuh, T. The anode performance of the hard carbon for the lithium ion battery derived from the oxygen-containing aromatic precursors. *J. Power Sources* **2010**, *195*, 7452–7456. [CrossRef]
36. Stan, A.I.; Swierczynski, M.; Stroe, D.I.; Teodorescu, R.; Andreasen, S.J. Lithium ion battery chemistries from renewable energy storage to automotive and back-up power applications—An overview. In Proceedings of the 2014 IEEE International Conference on Optimization of Electrical and Electronic Equipment (OPTIM), Brasov, Romania, 22–24 May 2014; pp. 713–720.
37. Kwon, T.-W.; Choi, J.W.; Coskun, A. Prospect for Supramolecular Chemistry in High-Energy-Density Rechargeable Batteries. *Joule* **2019**, *3*, 662–682. [CrossRef]
38. Link, S.; Neef, C.; Wicke, T. Trends in Automotive Battery Cell Design: A Statistical Analysis of Empirical Data. *Batteries* **2023**, *9*, 261. [CrossRef]
39. Löbberding, H.; Wessel, S.; Offermanns, C.; Kehrer, M.; Rother, J.; Heimes, H.; Kampker, A. From Cell to Battery System in BEVs: Analysis of System Packing Efficiency and Cell Types. *World Electr. Veh. J.* **2020**, *11*, 77. [CrossRef]
40. Hummes, D.N.; Hunt, J.; Hervé, B.B.; Schneider, P.S.; Montanari, P.M. A comparative study of different battery geometries used in electric vehicles. *Lat. Am. J. Energy Res.* **2023**, *10*, 94–114. [CrossRef]
41. Hannan, M.A.; Hoque, M.M.; Hussain, A.; Yusof, Y.; Ker, P.J. State-of-the-art and energy management system of lithium-ion batteries in electric vehicle applications: Issues and recommendations. *IEEE Access* **2018**, *6*, 19362–19378. [CrossRef]
42. Miao, Y.; Hynan, P.; Von Jouanne, A.; Yokochi, A. Current Li-ion battery technologies in electric vehicles and opportunities for advancements. *Energies* **2019**, *12*, 1074. [CrossRef]
43. Kharabati, S.; Saedodin, S. A systematic review of thermal management techniques for electric vehicle batteries. *J. Energy Storage* **2024**, *75*, 109586. [CrossRef]
44. Bugryniec, P.J.; Resendiz, E.G.; Nwophoke, S.M.; Khanna, S.; James, C.; Brown, S.F. Review of gas emissions from lithium-ion battery thermal runaway failure—Considering toxic and flammable compounds. *J. Energy Storage* **2024**, *87*, 111288. [CrossRef]
45. Sarasketa-Zabala, E.; Gandiaga, I.; Rodriguez-Martinez, L.M.; Villarreal, I. Calendar ageing analysis of a $LiFePO_4$/graphite cell with dynamic model validations: Towards realistic lifetime predictions. *J. Power Sources* **2014**, *272*, 45–57. [CrossRef]
46. Naumann, M.; Schimpe, M.; Keil, P.; Hesse, H.C.; Jossen, A. Analysis and modeling of calendar aging of a commercial $LiFePO_4$/graphite cell. *J. Energy Storage* **2018**, *17*, 153–169. [CrossRef]
47. Keil, P.; Jossen, A. Calendar Aging of NCA Lithium-Ion Batteries Investigated by Differential Voltage Analaysis and Coulomb Tracking. *J. Electrochem. Soc.* **2017**, *164*, A6066–A6074. [CrossRef]
48. Schmitt, J.; Maheshwari, A.; Heck, M.; Lux, S.; Vetter, M. Impedance change and capacity fade of lithium nickel manganese cobalt oxide-based batteries during calendar aging. *J. Power Sources* **2017**, *353*, 183–194. [CrossRef]
49. Deng, Z.; Xu, L.; Liu, H.; Hu, X.; Duan, Z.; Xu, Y. Prognostics of battery capacity based on charging data and data-driven methods for on-road vehicles. *Appl. Energy* **2023**, *339*, 120954. [CrossRef]
50. Birkl, C.R.; Roberts, M.R.; McTurk, E.; Bruce, P.G.; Howey, D.A. Degradation diagnostics for lithium ion cells. *J. Power Sources* **2017**, *341*, 373–386. [CrossRef]
51. Chen, Y.; Torres-Castro, L.; Chen, K.-H.; Penley, D.; Lamb, J.; Karulkar, M.; Dasgupta, N.P. Operando detection of Li plating during fast charging of Li-ion batteries using incremental capacity analysis. *J. Power Sources* **2022**, *539*, 231601. [CrossRef]
52. Vikrant, K.S.N.; Allu, S. Modeling of Lithium Nucleation and Plating Kinetics Under Fast Charge Conditions. *J. Electrochem. Soc.* **2021**, *168*, 020536. [CrossRef]
53. Gailani, A.; Mokidm, R.; El-Dalahmeh, M.; El-Dalahmeh, M.; Al-Greer, M. Analysis of Lithium-ion Battery Cells Degradation Based on Different Manufacturers. In Proceedings of the 55th International Universities Power Engineering Conference (UPEC), Turin, Italy, 1–4 September 2020; pp. 1–6. [CrossRef]
54. Hao, Y.; Li, K.; Zhang, S.; Wang, J.; Zhu, X.; Meng, W.; Qiu, J.; Ming, H. Failure of Lithium-Ion Batteries Accelerated by Gravity. *ACS Appl. Mater. Interfaces* **2024**, *16*, 27400–27409. [CrossRef]
55. Wang, S.; Wu, T.; Xie, H.; Li, C.; Zhang, J.; Jiang, L.; Wang, Q. Effects of Current and Ambient Temperature on Thermal Response of Lithium Ion Battery. *Batteries* **2022**, *8*, 203. [CrossRef]
56. Liu, X.M.; Arnold, C.B. Effects of Current Density on Defect-Induced Capacity Fade through Localized Plating in Lithium-Ion Batteries. *J. Electrochem. Soc.* **2020**, *167*, 130519. [CrossRef]
57. Barcellona, S.; Piegari, L. Effect of current on cycle aging of lithium ion batteries. *J. Energy Storage* **2020**, *29*, 101310. [CrossRef]
58. Xu, R.; Yang, Y.; Yin, F.; Liu, P.; Cloetens, P.; Liu, Y.; Lin, F.; Zhao, K. Heterogeneous damage in Li-ion batteries: Experimental analysis and theoretical modeling. *J. Mech. Phys. Solids* **2019**, *129*, 160–183. [CrossRef]
59. Ai, W.; Kraft, L.; Sturm, J.; Jossen, A.; Wu, B. Electrochemical thermal-mechanical modelling of stress inhomogeneity in lithium-ion pouch cells. *J. Electrochem. Soc.* **2020**, *167*, 013512. [CrossRef]

60. Wang, R.; Zhou, X.; Wang, Y.; Xiao, Y.; Shi, Z.; Liu, Y.; Zhang, T. Degradation analysis of lithium-ion batteries under ultrahigh-rate discharge profile. *Appl. Energy* **2024**, *376*, 124241. [CrossRef]
61. Wang, D.; Wu, X.; Wang, Z.; Chen, L. Cracking causing cyclic instability of $LiFePO_4$ cathode material. *J. Power Sources* **2005**, *140*, 125–128. [CrossRef]
62. Lim, M.-R.; Cho, W.-I.; Kim, K.-B. Preparation and characterization of gold-codeposited $LiMn_2O_4$ electrodes. *J. Power Sources* **2001**, *92*, 168–176. [CrossRef]
63. Wang, H.; Jang, Y.-I.; Huang, B.; Sadoway, D.R.; Chiang, Y.-M. TEM study of electrochemical cycling-induced damage and disorder in $LiCoO_2$ cathodes for rechargeable lithium batteries. *J. Electrochem. Soc.* **1999**, *146*, 473–480. [CrossRef]
64. Zhu, M.; Park, J.; Sastry, A.M. Fracture Analysis of the Cathode in Li-Ion Batteries: A Simulation Study. *J. Electrochem. Soc.* **2012**, *4*, 492–498. [CrossRef]
65. Savoye, F.; Venet, P.; Millet, M.; Groot, J. Impact of periodic current pulses on li-ion battery performance. *IEEE Trans. Ind. Electron.* **2012**, *59*, 3481–3488. [CrossRef]
66. Lee, Y.-D.; Park, S.-Y. Electrochemical state-based sinusoidal ripple current charging control. *IEEE Trans. Power Electron.* **2015**, *30*, 4232–4243. [CrossRef]
67. Abdel-Monem, M.; Trad, K.; Omar, N.; Hegazy, O.; den Bossche, P.V.; Mierlo, J.V. Influence analysis of static and dynamic fast-charging current profiles on ageing performance of commercial lithiumion batteries. *Energy* **2017**, *120*, 179–191. [CrossRef]
68. Monem, M.A.; Trad, K.; Omar, N.; Hegazy, O.; Mantels, B.; Mulder, G.; Van den Bossche, P.; Van Mierlo, J. Lithium-ion batteries: Evaluation study of different charging methodologies based on aging process. *Appl. Energy* **2015**, *152*, 143–155. [CrossRef]
69. Keil, P.; Jossen, A. Charging protocols for lithium-ion batteries and their impact on cycle life—An experimental study with different 18650 high-power cells. *J. Energy Storage* **2016**, *6*, 125–141. [CrossRef]
70. Uno, M.; Tanaka, K. Influence of high-frequency charge–discharge cycling induced by cell voltage equalizers on the life performance of lithium-ion cells. *IEEE Trans. Veh. Technol.* **2011**, *60*, 1505–1515. [CrossRef]
71. Li, J.; Murphy, E.; Winnick, J.; Kohl, P.A. The effects of pulse charging on cycling characteristics of commercial lithium-ion batteries. *J. Power Sources* **2001**, *102*, 302–309. [CrossRef]
72. Cho, S.-Y.; Lee, I.-O.; Baek, J.-I.; Moon, G.-W. Battery Impedance Analysis Considering DC Component in Sinusoidal Ripple-Current Charging. *IEEE Trans. Ind. Electron.* **2015**, *63*, 1561–1573. [CrossRef]
73. Chen, L.-R.; Wu, S.-L.; Shieh, D.-T.; Chen, T.-R. Sinusoidal-Ripple-Current Charging Strategy and Optimal Charging Frequency Study for Li-Ion Batteries. *IEEE Trans. Ind. Electron.* **2013**, *60*, 88–97. [CrossRef]
74. Bessman, A.; Soares, R.; Wallmark, O.; Svens, P.; Lindbergh, G. Aging effects of AC harmonics on lithium-ion cells. *J. Energy Storage* **2019**, *21*, 741–749. [CrossRef]
75. Kannan, D.R.R.; Weatherspoon, M.H. The effect of pulse charging on commercial lithium nickel cobalt oxide (NMC) cathode lithium-ion batteries. *J. Power Sources* **2020**, *479*, 229085. [CrossRef]
76. Bessman, A.; Soares, R.; Vadivelu, S.; Wallmark, O.; Svens, P.; Ekstrom, H.; Lindbergh, G. Challenging sinusoidal ripple-current charging of lithium-ion batteries. *IEEE Trans. Ind. Electron.* **2018**, *65*, 4750–4757. [CrossRef]
77. Huang, X.; Liu, W.; Acharya, A.B.; Meng, J.; Teodorescu, R.; Stroe, D.-I. Effect of Pulsed Current on Charging Performance of Lithium-ion Batteries. *IEEE Trans. Ind. Electron.* **2022**, *69*, 10144–10153. [CrossRef]
78. Althurthi, S.B.; Rajashekara, K.; Debnath, T. Comparison of EV Fast Charging Protocols and Impact of Sinusoidal Half-Wave Fast Charging Methods on Lithium-Ion Cells. *World Electr. Veh. J.* **2024**, *15*, 54. [CrossRef]
79. Lv, H.; Huang, X.; Liu, Y. Analysis on pulse charging–discharging strategies for improving capacity retention rates of lithium-ion batteries. *Ionics* **2020**, *26*, 1749–1770. [CrossRef]
80. Guo, J.; Xu, Y.; Exner, M.; Huang, X.; Li, Y.; Liu, Y.; Wang, H.; Kowal, J.; Zhang, Q.; Kristensen, P.K.; et al. Unravelling the Mechanism of Pulse Current Charging for Enhancing the Stability of Commercial $LiNi_{0.5}Mn_{0.3}Co_{0.2}O_2$/Graphite Lithium-Ion Batteries. *Adv. Energy Mater.* **2024**, *14*, 2400190. [CrossRef]
81. Aryanfar, A.; Brooks, D.; Merinov, B.V.; Goddard, W.A., III; Colussi, A.J.; Hoffmann, M.R. Dynamics of lithium dendrite growth and inhibition: Pulse charging experiments and Monte Carlo calculations. *J. Phys. Chem. Lett.* **2014**, *5*, 1721–1726. [CrossRef] [PubMed]
82. Schneider, N.M.; Park, J.H.; Grogan, J.M.; Steingart, D.A.; Bau, H.H.; Ross, F.M. Nanoscale evolution of interface morphology during electrodeposition. *Nat. Commun.* **2017**, *8*, 2174. [CrossRef]
83. Mayers, M.Z.; Kaminski, J.W.; Miller, T.F., III. Suppression of dendrite formation via pulse charging in rechargeable lithium metal batteries. *J. Phys. Chem.* **2012**, *116*, 26214–26221. [CrossRef]
84. Reisecker, V.; Flatscher, F.; Porz, L.; Fincher, C.; Todt, J.; Hanghofer, I.; Hennige, V.; Linares-Moreau, M.; Falcaro, P.; Ganschow, S.; et al. Effect of pulse-current-based protocols on the lithium dendrite formation and evolution in all-solid-state batteries. *Nat. Commun.* **2023**, *14*, 2432. [CrossRef]
85. Qu, Z.G.; Jiang, Z.Y.; Wang, Q. Experimental study on pulse self–heating of lithium–ion battery at low temperature. *Int. J. Heat Mass Transf.* **2019**, *135*, 696–705. [CrossRef]

86. Li, L.; Basu, S.; Wang, Y.; Chen, Z.; Hundekar, P.; Wang, B.; Shi, J.; Shi, Y.; Narayanan, S.; Koratkar, N. Self-heating–induced healing of lithium dendrites. *Science* **2018**, *359*, 1513–1516. [CrossRef] [PubMed]
87. Huang, X.; Li, Y.; Acharya, A.B.; Sui, X.; Meng, J.; Teodorescu, R.; Stroe, D.-I. A Review of Pulsed Current Technique for Lithium-ion Batteries. *Energies* **2020**, *13*, 2458. [CrossRef]
88. Zhao, Y.; Lu, B.; Song, Y.; Zhang, J. A modified pulse charging method for lithium-ion batteries by considering stress evolution, charging time and capacity utilization. *Front. Struct. Civ. Eng.* **2019**, *13*, 294–302. [CrossRef]
89. Jiang, Z.; Dougal, R.A. Synergetic control of power converters for pulse current charging of advanced batteries from a fuel cell power source. *IEEE Trans. Power Electron.* **2004**, *19*, 1140–1150. [CrossRef]
90. Purushothaman, B.K.; Morrison, P.W., Jr.; Landau, U. Reducing Mass-Transport Limitations by Application of Special Pulsed Current Modes. *J. Electrochem. Soc.* **2005**, *152*, J33. [CrossRef]
91. Che, Y.; Stroe, D.-I.; Sui, X.; Vilsen, S.B.; Hu, X.; Teodorescu, R. Battery Aging Behavior Evaluation under Variable and Constant Temperatures with Real Loading Profiles. In Proceedings of the IEEE Applied Power Electronics Conference and Exposition (APEC), Orlando, FL, USA, 19–23 March 2023; pp. 2979–2983. [CrossRef]
92. Kalk, A.; Holocher, M.C.; Ohneseit, S.; Kupper, C.; Hiller, M. Effects of Realistic Driving Profiles on the Degradation of Lithium-Ion Batteries. In Proceedings of the 2023 IEEE International Transportation Electrification Conference (ITEC-India), Chennai, India, 12–15 December 2023. [CrossRef]
93. Brand, M.J.; Hofmann, M.H.; Schuster, S.S.; Keil, P.; Jossen, A. The influence of current ripples on the life-time of lithium-ion batteries. *IEEE Trans. Veh. Technol.* **2018**, *67*, 10438–10445. [CrossRef]
94. Bala, S.; Tengnér, T.; Rosenfeld, P.; Delince, F. The effect of low frequency current ripple on the performance of a Lithium Iron Phosphate (LFP) battery energy storage system. In Proceedings of the IEEE Energy Conversion Congress and Exposition (ECCE), Raleigh, NC, USA, 15–20 September 2012; pp. 3485–3492. [CrossRef]
95. Bellache, K.; Camara, M.B.; Dakyo, B.; Sridhar, R. Aging Characterization of Lithium Iron Phosphate Batteries considering Temperature and Direct Current Undulations as Degrading factors. *IEEE Trans. Ind. Electron.* **2020**, *68*, 9696–9706. [CrossRef]
96. Beh, H.Z.Z.; Covic, G.A.; Boys, J.T. Effects of pulse and DC charging on lithium iron phosphate ($LiFePO_4$) batteries. In Proceedings of the IEEE Energy Conversion Congress and Exposition, Denver, CO, USA, 15–19 September 2013; pp. 315–320. [CrossRef]
97. Prasad, R.; Namuduri, C.; Kollmeyer, P. Onboard Unidirectional Automotive G2V Battery Charger using Sine Charging and its Effect on Li-ion Batteries. In Proceedings of the 2015 IEEE Energy Conversion Congress and Exposition (ECCE), Montreal, QC, Canada, 20–24 September 2015. [CrossRef]
98. De Breucker, S.; Engelen, K.; D'hulst, R.; Driesen, J. Impact of current ripple on Li-ion battery ageing. *World Electr. Veh. J.* **2013**, *6*, 532–540. [CrossRef]
99. Uddin, K.; Moore, A.D.; Barai, A.; Marco, J. The effects of high frequency current ripple on electric vehicle battery performance. *Appl. Energy* **2016**, *178*, 142–154. [CrossRef]
100. Uddin, K.; Somerville, L.; Barai, A.; Lain, M.; Ashwin, T.R.; Jennings, P.; Marco, J. The impact of high-frequency-high-current perturbations on film formation at the negative electrode-electrolyte interface. *Electrochim. Acta* **2017**, *233*, 1–12. [CrossRef]
101. Goldammer, E.; Gentejohann, M.; Schlüter, M.; Weber, D.; Wondrak, W.; Dieckerhoff, S.; Gühmann, C.; Kowal, J. The Impact of an Overlaid Ripple Current on Battery Aging: The Development of the SiCWell Dataset. *Batteries* **2022**, *8*, 11. [CrossRef]
102. Ferraz, P.K.P.; Kowal, J. A Comparative Study on the Influence of DC/DC-Converter Induced High Frequency Current Ripple on Lithium-Ion Batteries. *Sustainability* **2019**, *11*, 6050. [CrossRef]
103. Chang, F.; Roemer, F.; Lienkamp, M. Influence of Current Ripples in Cascaded Multilevel Topologies on the Aging of Lithium Batteries. *IEEE Trans. Power Electron.* **2020**, *35*, 11879–11890. [CrossRef]
104. Frenander, K.; Thiringer, T. Low Frequency influence on degradation of commercial Li-ion battery. *Electrochim. Acta* **2023**, *462*, 142760. [CrossRef]
105. Li, H.; Zhang, W.; Sun, B.; Cai, X.; Fan, X.; Zhao, B.; Zhang, C. The degradation characteristics and mechanism of $Li[Ni_{0.5}Co_{0.2}Mn_{0.3}]O_2$ batteries with high frequency current ripple excitation. *Appl. Energy* **2023**, *343*, 121242. [CrossRef]
106. Ghassemi, A.; Banerjee, P.C.; Hollenkamp, A.F.; Zhang, Z.; Bahrani, B. Effects of alternating current on Li-ion battery performance: Monitoring degradative processes with in-situ characterization techniques. *Appl. Energy* **2021**, *284*, 116192. [CrossRef]
107. Hu, X.; Zhang, K.; Liu, K.; Lin, X.; Dey, S.; Onori, S. Advanced fault diagnosis for lithium-ion battery systems: A review of fault mechanisms, fault features, and diagnosis procedures. *IEEE Ind. Electron. Mag.* **2020**, *14*, 65–91. [CrossRef]
108. Elmahallawy, M.; Elfouly, T.; Alouani, A.; Massoud, A.M. A Comprehensive Review of Lithium-Ion Batteries Modeling, and State of Health and Remaining Useful Lifetime Prediction. *IEEE Access* **2022**, *10*, 119040–119070. [CrossRef]
109. Li, Y.; Liu, K.; Foley, A.M.; Zülke, A.; Berecibar, M.; Nanini-Maury, E.; Van Mierlo, J.; Hoster, H.E. Data-driven health estimation and lifetime prediction of lithium-ion batteries: A review. *Renew. Sustain. Energy Rev.* **2019**, *113*, 109254. [CrossRef]
110. Zou, B.; Zhang, L.; Xue, X.; Tan, R.; Jiang, P.; Ma, B.; Song, Z.; Hua, W. A Review on the Fault and Defect Diagnosis of Lithium-Ion Battery for Electric Vehicles. *Energies* **2023**, *16*, 5507. [CrossRef]

111. Li, C.; Liu, X.; Wang, C.; Ye, L.; Wu, T.; Liang, Z.; Zhang, Z.; Zeng, Y.; Li, K. Electrochemical-thermal behaviors of retired power lithium-ion batteries during high-temperature and overcharge/over-discharge cycles. *Case Stud. Therm. Eng.* **2024**, *61*, 104898. [CrossRef]
112. Guo, R.; Lu, L.; Ouyang, M.; Feng, X. Mechanism of the entire overdischarge process and overdischarge-induced internal short circuit in lithium-ion batteries. *Sci. Rep.* **2016**, *6*, 30248. [CrossRef] [PubMed]
113. Erol, S. Equivalent Circuit Model for Electrochemical Impedance Spectroscopy of Commercial 18650 Lithium-Ion Cell Under Over-Discharge and Overcharge Conditions. *Electroanalysis* **2024**, *36*, e202300232. [CrossRef]
114. Gotz, J.D.; Teixeira, M.A.S.; Correa, F.C.; Viana, E.R.; Badin, A.A.; Borsato, M. The Influence of Overcharging and Over-Discharging on the Capacity Degradation of Lithium-Ion Batteries. In Proceedings of the 2024 IEEE Vehicle Power and Propulsion Conference (VPPC), Washington, DC, USA, 7–10 October 2024; pp. 1–6. [CrossRef]
115. Millner, A. Modeling lithium ion battery degradation in electric vehicles. In Proceedings of the 2010 IEEE Conference on Innovative Technologies for an Efficient and Reliable Electricity Supply, Waltham, MA, USA, 27–29 September 2010; pp. 349–356. [CrossRef]
116. Zhang, S.; Hosen, M.S.; Kalogiannis, T.; Van Mierlo, J.; Berecibar, M. State of Health Estimation of Lithium-Ion Batteries Based on Electrochemical Impedance Spectroscopy and Backpropagation Neural Network. *World Electr. Veh. J.* **2021**, *12*, 156. [CrossRef]
117. Chowdhury, N.R.; Smith, A.J.; Frenander, K.; Mikheenkova, A.; Lindström, R.W.; Thiringer, T. Influence of state of charge window on the degradation of Tesla lithium-ion battery cells. *J. Energy Storage* **2024**, *76*, 110001. [CrossRef]
118. Zhong, H.; Zhong, Q.; Yang, J.; Zhong, S. Thermal behavior and failure mechanisms of 18650 lithium ion battery induced by overcharging cycling. *Energy Rep.* **2022**, *8*, 7286–7296. [CrossRef]
119. Peng, Y.; Yang, L.; Ju, X.; Liao, B.; Ye, K.; Li, L.; Cao, B.; Ni, Y. A Comprehensive Investigation on the Thermal and Toxic Hazards of Large Format Lithium-ion Batteries with $LiFePO_4$ Cathode. *J. Hazard. Mater.* **2020**, *381*, 120916. [CrossRef]
120. Wikner, E.; Bjorklund, E.; Fridner, J.; Brandell, D.; Thiringer, T. How the utilised SOC window in commercial Li-ion pouch cells influence battery ageing. *J. Power Sources Adv.* **2021**, *8*, 100054. [CrossRef]
121. Pelletier, S.; Jabali, O.; Laporte, G.; Veneroni, M. Battery Degradation and Behaviour for Electric Vehicles: Review and Numerical Analysis of Several Models. *Transp. Res. B Methodol.* **2017**, *103*, 158–187. [CrossRef]
122. Xu, B.; Oudalov, A.; Ulbig, A.; Andersson, G.; Kirschen, D.S. Modeling of Lithium-Ion Battery Degradation for Cell Life Assessment. *IEEE Trans. Smart Grid* **2016**, *9*, 1131–1140. [CrossRef]
123. Keil, P.; Schuster, S.; Wilhelm, J.; Travi, J.; Hauser, A.; Karl, R.C.; Jossen, A. Calendar Aging of Lithium-Ion Batteries. *J. Electrochem. Soc.* **2016**, *163*, A1872–A1880. [CrossRef]
124. Geisbauer, C.; Wöhrl, K.; Koch, D.; Wilhelm, G.; Schneider, G.; Schweiger, H.-G. Comparative Study on the Calendar Aging Behavior of Six Different Lithium-Ion Cell Chemistries in Terms of Parameter Variation. *Energies* **2021**, *14*, 3358. [CrossRef]
125. Väyrynen, A.; Salminen, J. Lithium ion battery production. *J. Chem. Thermodyn.* **2012**, *46*, 80–85. [CrossRef]
126. Bandhauer, T.M.; Garimella, S.; Fuller, T.F. A Critical Review of Thermal Issues in Lithium-Ion Batteries. *J. Electrochem. Soc.* **2011**, *3*, R1–R25. [CrossRef]
127. Spitthoff, L.; Shearing, P.R.; Burheim, O.S. Temperature, Ageing and Thermal Management of Lithium-Ion Batteries. *Adv. Technol. Improv. Energy Effic. Storage* **2021**, *14*, 1248. [CrossRef]
128. Zhu, J.; Sun, Z.; Wei, X.; Dai, H.; Gu, W. Experimental investigations of AC pulse heating method for vehicular high power lithium-ion batteries at subzero temperatures. *J. Power Sources* **2017**, *367*, 145–157. [CrossRef]
129. Herreyre, S.; Huchet, O.; Barusseau, S.; Perton, F.; Bodet, J.; Biensan, P. New Li-ion electrolytes for low temperature applications. *J. Power Sources* **2001**, *97*, 576–580. [CrossRef]
130. Zhang, N.; Deng, T.; Zhang, S.; Wang, C.; Chen, L.; Wang, C.; Fan, X. Critical review on low-temperature Li-ion/metal batteries. *Adv. Mater.* **2022**, *34*, 2107899. [CrossRef]
131. Hou, J.; Yang, M.; Wang, D.; Zhang, J. Fundamentals and challenges of lithium ion batteries at temperatures between −40 and 60 °C. *Adv. Energy Mater.* **2020**, *10*, 1904152. [CrossRef]
132. Weng, S.; Zhang, X.; Yang, G.; Zhang, S.; Ma, B.; Liu, Q.; Liu, Y.; Peng, C.; Chen, H.; Yu, H.; et al. Temperature-dependent interphase formation and Li^+ transport in lithium metal batteries. *Nat. Commun.* **2023**, *14*, 4474. [CrossRef]
133. Tran, M.-K.; Mathew, M.; Janhunen, S.; Panchal, S.; Raahemifar, K.; Fraser, R.; Fowler, M. A comprehensive equivalent circuit model for lithium-ion batteries, incorporating the effects of state of health, state of charge, and temperature on model parameters. *J. Energy Storage* **2021**, *43*, 103252. [CrossRef]
134. Ouyang, D.; He, Y.; Weng, J.; Liu, J.; Chen, M.; Wang, J. Influence of low temperature conditions on lithium-ion batteries and the application of an insulation material. *RSC Adv.* **2019**, *9*, 9053–9066. [CrossRef]
135. Lecompte, M.; Bernard, J.; Calas, E.; Richardet, L.; Guignard, A.; Duclaud, F.; Voyer, D.; Montaru, M.; Crouzevialle, B.; Lonardoni, L.; et al. Experimental assessment of high-energy high nickel-content NMC lithium-ion battery cycle life at cold temperatures. *J. Energy Storage* **2024**, *94*, 112443. [CrossRef]

136. Petzl, M.; Kasper, M.; Danzer, M.A. Lithium plating in a commercial lithium-ion battery—A low-temperature aging study. *J. Power Sources* **2015**, *275*, 799–807. [CrossRef]
137. Lu, Y.; Zhao, C.-Z.; Yuan, H.; Cheng, X.-B.; Huang, J.-Q.; Zhang, Q. Critical Current Density in Solid-State Lithium Metal Batteries: Mechanism, Influences, and Strategies. *Adv. Funct. Mater.* **2021**, *31*, 2009925. [CrossRef]
138. Lu, Y.; Huang, X.; Song, Z.; Rui, K.; Wang, Q.; Gu, S.; Yang, J.; Xiu, T.; Badding, M.E.; Wen, Z. Highly stable garnet solid electrolyte based Li-S battery with modified anodic and cathodic interfaces. *Energy Storage Mater.* **2018**, *15*, 282–290. [CrossRef]
139. Yu, S.; Siegel, D.J. Grain Boundary Softening: A Potential Mechanism for Lithium Metal Penetration through Stiff Solid Electrolytes. *ACS Appl. Mater. Interfaces* **2018**, *10*, 38151–38158. [CrossRef] [PubMed]
140. Ping, W.; Wang, C.; Lin, Z.; Hitz, E.; Yang, C.; Wang, H.; Hu, L. Reversible Short-Circuit Behaviors in Garnet-Based Solid-State Batteries. *Adv. Energy Mater.* **2020**, *10*, 2000702. [CrossRef]
141. Werner, D.; Paarmann, S.; Wetzel, T. Calendar Aging of Li-Ion Cells—Experimental Investigation and Empirical Correlation. *Batteries* **2021**, *7*, 28. [CrossRef]
142. Ali, H.; Beltran, H.; Lindsey, N.J.; Pecht, M. Assessment of the calendar aging of lithium-ion batteries for a long-term—Space missions. *Front. Energy Res.* **2023**, *11*, 1108269. [CrossRef]
143. Duan, J.; Tang, X.; Dai, H.; Yang, Y.; Wu, W.; Wei, X.; Huang, Y. Building Safe Lithium-Ion Batteries for Electric Vehicles: A Review. *Electrochem. Energy Rev.* **2020**, *3*, 1–42. [CrossRef]
144. Maleki, H.; Deng, G.; Anani, A.; Howard, J. Thermal stability studies of Li-ion cells and components. *J. Electrochem. Soc.* **1999**, *146*, 3224. [CrossRef]
145. Li, J.; Huang, J.; Cao, M. Properties enhancement of phase-change materials via silica and Al honeycomb panels for the thermal management of $LiFeO_4$ batteries. *Appl. Therm Eng.* **2018**, *131*, 660–668. [CrossRef]
146. Ohneseit, S.; Finster, P.; Floras, C.; Lubenau, N.; Uhlmann, N.; Seifert, H.J.; Ziebert, C. Thermal and Mechanical Safety Assessment of Type 21700 Lithium-Ion Batteries with NMC, NCA and LFP Cathodes–Investigation of Cell Abuse by Means of Accelerating Rate Calorimetry (ARC). *Batteries* **2023**, *9*, 237. [CrossRef]
147. Brand, M.; Gläser, S.; Geder, J.; Menacher, S.; Obpacher, S.; Jossen, A.; Quinger, D. Electrical safety of commercial Li-ion cells based on NMC and NCA technology compared to LFP technology. In Proceedings of the EVS27 International Battery, Hybrid and Fuel Cell Electric Vehicle Symposium, Barcelona, Spain, 17–20 November 2013; pp. 1–9. [CrossRef]
148. Gao, T.; Bai, J.; Ouyang, D.; Wang, Z.; Bai, W.; Mao, N.; Zhu, Y. Effect of aging temperature on thermal stability of lithium-ion batteries: Part A—High-temperature aging. *Renew. Energy* **2023**, *203*, 592–600. [CrossRef]
149. Huang, Y.; Lu, S.; Zhu, S.; Su, M.; Yang, S.; Zeng, W.; Zhan, H.; Yang, Y.; Mei, J. Failure mechanisms of the $Li(Ni_{0.6}Co_{0.2}Mn_{0.2})O_2$-$Li_4Ti_5O_{12}$ lithium-ion batteries in long-time high rate cycle. *RSC Adv.* **2024**, *14*, 13592–13604. [CrossRef] [PubMed]
150. Han, X.; Xia, S.; Cao, J.; Wang, C.; Chen, M.-g. Effect of Humidity on Properties of Lithium-ion Batteries. *Int. J. Electrochem. Sci.* **2021**, *16*, 210554. [CrossRef]
151. Byun, S.; Park, J.; Appiah, W.A.; Ryou, M.-H.; Lee, Y.M. The effects of humidity on the self-discharge properties of $Li(Ni_{1/3}Co_{1/3}Mn_{1/3})O_2$/graphite and $LiCoO_2$/graphite lithium-ion batteries during storage. *RSC Adv.* **2017**, *7*, 10915–10921. [CrossRef]
152. Zhang, L.; Gubler, E.A.M.; Tai, C.-W.; Kondracki, Ł.; Sommer, H.; Novák, P.; El Kazzi, M.; Trabesinger, S. Elucidating the Humidity-Induced Degradation of Ni-Rich Layered Cathodes for Li-Ion Batteries. *ACS Appl. Mater. Interfaces* **2022**, *14*, 13240–13249. [CrossRef]
153. Fullerton-Shirey, S.K.; Ganapatibhotla, L.V.N.R.; Shi, W.; Maranas, J.K. Influence of Thermal History and Humidity on the Ionic Conductivity of Nanoparticle-Filled Solid Polymer Electrolytes. *J. Polym. Sci. Part B Polym. Phys.* **2011**, *49*, 1496–1505. [CrossRef]
154. Zhou, M.; Hu, L.; Chen, S.; Zhao, X. Different mechanical-electrochemical coupled failure mechanism and safety evaluation of lithium-ion pouch cells under dynamic and quasi-static mechanical abuse. *J. Power Sources* **2021**, *497*, 229897. [CrossRef]
155. Wang, R.; Liu, G.; Wang, C.; Ji, Z.; Yu, Q. A comparative study on mechanical-electrical-thermal characteristics and failure mechanism of LFP/NMC/LTO batteries under mechanical abuse. *eTransportation* **2024**, *22*, 100359. [CrossRef]
156. An, Z.; Shi, T.; Du, X.; An, X.; Zhang, D.; Bai, J. Experimental study on the internal short circuit and failure mechanism of lithium-ion batteries under mechanical abuse conditions. *J. Energy Storage* **2024**, *89*, 111819. [CrossRef]
157. Aiello, L.; Ruchti, P.; Vitzthum, S.; Coren, F. Influence of Pressure, Temperature and Discharge Rate on the Electrical Performances of a Commercial Pouch Li-Ion Battery. *Batteries* **2024**, *10*, 72. [CrossRef]
158. Lelie, M.; Braun, T.; Knips, M.; Nordmann, H.; Ringbeck, F.; Zappen, H.; Sauer, D.U. Battery Management System Hardware Concepts: An Overview. *Appl. Sci.* **2018**, *8*, 534. [CrossRef]
159. Andrea, D. *Battery Management Systems for Large Lithium-Ion Battery Packs*; Artech House: Norwood, MA, USA, 2010.
160. See, K.W.; Wang, G.; Zhang, Y.; Wang, Y.; Meng, L.; Gu, X.; Zhang, N.; Lim, K.C.; Zhao, L.; Xie, B. Critical review and functional safety of a battery management system for large-scale lithium-ion battery pack technologies. *Int. J. Coal Sci. Technol.* **2022**, *9*, 36. [CrossRef]

161. Krishna, T.N.V.; Kumar, S.V.S.V.P.D.; Srinivasa Rao, S.; Chang, L. Powering the Future: Advanced Battery Management Systems (BMS) for Electric Vehicles. *Energies* **2024**, *17*, 3360. [CrossRef]
162. Yang, Z.; Dong, Y.; Liu, C.; Feng, X.; Jin, H.; Ma, X.; Ding, F.; Li, B.; Bai, L.; Ouyang, Y.; et al. Design and synthesis of high-silicon silicon suboxide nanowires by radio-frequency thermal plasma for high-performance lithium-ion battery anodes. *Appl. Surf. Sci.* **2023**, *614*, 156235. [CrossRef]
163. Zhao, R.; Liu, J.; Gu, J. The effects of electrode thickness on the electrochemical and thermal characteristics of lithium ion battery. *Appl. Energy* **2015**, *139*, 220–229. [CrossRef]
164. Sievers, M.; Sievers, U.; Mao, S.S. Thermal modelling of new Li-ion cell design modifications. *Forsch Ingenieurwes* **2010**, *74*, 215–231. [CrossRef]
165. Shah, K.; Jain, A. Modeling of steady-state and transient thermal performance of a Li-ion cell with an axial fluidic channel for cooling. *Int. J. Energy Res.* **2015**, *39*, 573–584. [CrossRef]
166. Nyamathulla, S.; Dhanamjayulu, C. A review of battery energy storage systems and advanced battery management system for different applications: Challenges and recommendations. *J. Energy Storage* **2024**, *86*, 111179. [CrossRef]
167. Gabbar, H.A.; Othman, A.M.; Abdussami, M.R. Review of Battery Management Systems (BMS) Development and Industrial Standards. *Technologies* **2021**, *9*, 28. [CrossRef]
168. García, E.; Quiles, E.; Correcher, A. Distributed Intelligent Battery Management System Using a Real-World Cloud Computing System. *Sensors* **2023**, *23*, 3417. [CrossRef] [PubMed]
169. Kim, T.; Makwana, D.; Adhikaree, A.; Vagdoda, J.S.; Lee, Y. Cloud-based battery condition monitoring and fault diagnosis platform for large-scale lithium-ion battery energy storage systems. *Energies* **2018**, *11*, 125. [CrossRef]

Disclaimer/Publisher's Note: The statements, opinions and data contained in all publications are solely those of the individual author(s) and contributor(s) and not of MDPI and/or the editor(s). MDPI and/or the editor(s) disclaim responsibility for any injury to people or property resulting from any ideas, methods, instructions or products referred to in the content.